A novel approach for optimizing the natural gas liquefaction process

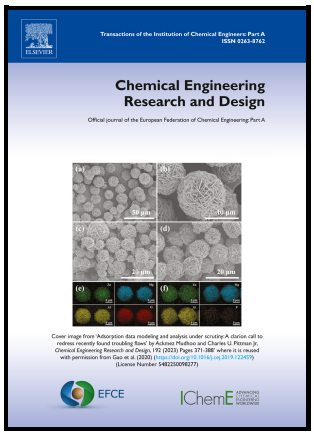

Juan I. Manassaldi, Jimena Incer-Valverde, Tatiana Morosuk, Sergio F. Mussati

PII: S0263-8762(24)00003-0

DOI: https://doi.org/10.1016/j.cherd.2024.01.003

Reference: CHERD6056

To appear in: *Chemical Engineering Research and Design*

Received date: 3 October 2023
Revised date: 30 December 2023
Accepted date: 2 January 2024

Please cite this article as: Juan I. Manassaldi, Jimena Incer-Valverde, Tatiana Morosuk and Sergio F. Mussati, A novel approach for optimizing the natural gas liquefaction process, *Chemical Engineering Research and Design,* (2024) doi:https://doi.org/10.1016/j.cherd.2024.01.003

A novel approach for optimizing the natural gas liquefaction process

Juan I. Manassaldi[1], Jimena Incer-Valverde[2], Tatiana Morosuk[2], Sergio F. Mussati[1,3]

[1] CAIMI Centro de Aplicaciones Informáticas y Modelado en Ingeniería (UTN–FRRo), Zeballos 1341, S2000BQA, Rosario, Argentina

[2] Institute for Energy Engineering, Technische Universität Berlin, Marchstr. 18, Berlin, Germany

[3] INGAR Instituto de Desarrollo y Diseño (CONICET-UTN), Avellaneda 3657, 3000, Santa Fe, Argentina

Abstract

The conversion of natural gas into liquefied natural gas (LNG) requires substantial energy consumption. This study proposes a deterministic mathematical model to find the optimal operation conditions for an LNG plant to minimize the energy consumption for turbomachinery and the total thermal conductance of the heat exchangers. General Algebraic Modeling System (GAMS) linked to a Dynamic Link Library was used to calculate the thermodynamic properties of the working fluids. A derivative-based optimization algorithm is used. Results indicate that the novel optimization approach allows the satisfactory management of the model nonlinearities associated, for example, with the bilinear terms involved in the energy balances and the mathematical functions used to calculate the thermodynamic properties. A preprocessing phase for initializing process variables is developed to facilitate model convergence. In comparison to an optimal design reported in the literature, which was obtained by integrating a well-established evolutionary optimization approach with the Aspen HYSYS simulator, the results indicated that the net electrical power could be reduced by up to 10% when the derivative-based optimization algorithm is used. The proposed deterministic approach, consisting of a mathematical model, an initialization phase, and an optimization algorithm, can help process engineers overcome the challenges associated with LNG process optimization.

Keywords: refrigeration, LNG, optimization, General Algebraic Modeling System optimization, deterministic mathematical model

1. Introduction

Natural gas (NG) serves as a crucial primary energy source on a global scale. The worldwide demand for liquefied natural gas (LNG) is rising because it is an efficient and market-flexible long-distance transportation (IEA, World Energy Outlook, 2022). Global gas demand is projected to increase by 140 billion cubic meters from 2021 to 2025 (IEA, Gas Market Report, Q3-2022). During the last decades, many countries have made substantial progress in developing medium and small-scale LNG facilities (IGU, World LNG report 2023).

LNG plants are characterized by high energy consumption, approximately 8% of the feed gas energy required for the liquefaction process. Dual nitrogen turbo-expanders and pre-cooled nitrogen expansion cycles are widely used among the various nitrogen expansion cycles. Numerous studies indicate that single mixed refrigerant (SMR) and nitrogen dual expander processes exhibit higher energy intensity (He et al., 2018; Khan et al., 2017). Consequently, substantial research efforts are currently on optimizing the size and operational parameters of LNG plants, intending to enhance their overall energetic efficiency (Qyyum et al., 2018a; He et al., 2018; Khan et al., 2017).

Complex computations to estimate highly nonlinear functions govern the thermodynamic properties of all working fluids involved in the LNG technology are addressed by many researchers (for example, Yoon et al., 2012). Furthermore, internal heat (cold) integration is a complex problem due to the internal loops of the working fluids within LNG refrigeration cycles. Similar problems are observed for improving the efficiency of other low-temperature or cryogenic processes is complicated without simultaneous optimization, e.g., the liquefaction of hydrogen (Incer-Valverde et al., 2023a), its regasification (Incer-Valverde et al., 2023b), and liquid air energy storage (Incer-Valverde et al., 2021), etc.

Numerous articles have reported optimizing LNG plants, focusing on combining evolutionary optimization algorithms with process simulators. For instance, the combination of genetic algorithms (GA) with ASPEN HYSYS has been discussed in many publications (Moein et al., 2015; Ding et al., 2016; Kahn et al. 2016; Jin and Lim, 2019; Cao et al. 2016; Yin and Ju, 2020; Almeida-Trasvina and Smith, 2019; Hu et al. 2021); GA with ASPEN Plus in (Primabudi et al., 2019; Xu et al. 2013), and GA with UniSim by Kim et al. 2023; Shin et al. 2015; and Khan and Lee, 2013. A detailed review of these publications is the following.

Moein et al. (2015) determined the optimal operational conditions for an SMR process to minimize energy consumption. The authors employed a genetic algorithm to minimize the total required work. Eleven variables were selected for the optimization procedure. In Yin and Lu (2020), the optimization of

two nitrogen expansion cycles within boil-off gas re-liquefaction systems, the parallel and serial nitrogen expansion processes, is reported. Applying a GA for optimization, the authors achieved a significant reduction in specific energy consumption, coefficient of performance (COP), and figure of merit for both processes compared to conventional approaches. Almeida-Trasvina and Smith (2019) report the investigation results of four small-scale SMR processes concerning energy efficiency improvement, incorporating structural changes to conventional PRICO and CryoMan processes. Aspen HYSYS was used for modeling and GA by MATLAB for optimization, achieving an 8.5% reduction in total energy demand compared to the commercial PRICO cycle. Also, by combining Aspen-HYSYS and MATLAB through Microsoft COM functionality, Khan et al. (2011), Khan et al. (2016) investigated a dual mixed refrigerant process of natural gas liquefaction consisting of two mixed refrigerant cycles: considering ethane and propane for the warm cycle, and nitrogen, methane, ethane, and propane for the cold cycle. A multi-objective optimization problem was investigated by simultaneously considering the specific compression energy and overall thermal conductance. The two objectives were encoded in Matlab to achieve the goal, and the state variables were taken from the Aspen HYSYS model through Microsoft Component Object Model (COM) functionality. By using the toolbox of "gamultiobj" in Matlab, the Pareto front for the two objective functions was generated. Other works that use the COM interface to communicate with Aspen-HYSYS with algebraic modeling languages for optimizing other processes are found in (Ruiz-Femenia et al. 2020, Forster et al. 2023). Primabudi et al. (2019) optimized the propane pre-cooled mixed refrigerant (C3MR) LNG process, adopting a multi-objective approach to exergy-based analysis to maximize exergy efficiency and minimize the total product cos. ASPEN Plus facilitated process simulation, while non-dominated sorting GA handled optimization. The total investment could be reduced by 18% at the expense of exergetic efficiency i.e., increasing the total exergy destruction by 38%. Khan and Lee (2013) applied the particle swarm optimization (PSO) method and UniSim to optimize the SMR process, successfully reducing compression energy. Their study demonstrated that the stochastic nature of PSO offers advantages in circumventing local optima and identifying feasible solutions. Also, the combination of PSO algorithms with Aspen HYSYS is reported by Qyyum et al. 2018b; Vikse et al. 2020; Ghorbani et al. 2014 as well as PSO with HYSYS by Brodal et al. 2019. The combination of Aspen HYSYS with Tabu Search and Nelder-Mead downhill simplex methods has been applied by Aspelund et al. (2010). Ghorbani et al. (2014) used the PSO approach in conjunction with nonlinear programming (NLP) techniques to optimize the parameters of mixed refrigerant cycles. They concluded that PSO has more advantages compared to NLP optimization techniques. In addition, some alternative combinations,

such as coupling Aspen HYSYS with GA followed by Sequential Quadratic Programming, are suggested by Hwang et al. (2013).

Evolutionary algorithms (EA) represent probabilistic procedures that depend on multiple control parameters for execution. While some control parameters are shared among various algorithms, each algorithm typically possesses its distinct set of control parameters (Lobo et al., 2007). For instance, GA incorporates the selection of operators and mutation probability, while particle swarm optimization relies on cognitive parameters and inertia weight. Should these parameters be inadequately configured, the algorithm may falter in finding a solution, resulting in a lack of model convergence. When an EA attains convergence, it often identifies favorable solutions; nevertheless, it cannot guarantee global optimality due to the inherent stochastic nature of its search method.

Furthermore, EAs can be computationally demanding when applied to extensive problems. This is attributable to the necessity to evaluate numerous candidate solutions and implement genetic operators, as shown in (Chen et al., 2017; Mehrpooya et al. 2017; Allahyarzadeh-Bidgoli et al. 2018). EAs find preference when addressing problems with discontinuities in model constraints and/or objective functions or when derivatives pose challenges or are unreliable to compute due to noise (Audet and Hare 2017). Conversely, despite process simulators featuring modules for diverse process units and bypassing the need for mathematical model development, their combination with evolutionary optimization algorithms retains EA-associated. These challenges involve the need for substantial effort and expertise in establishing and troubleshooting effective communication protocols between different software systems. Simulations can become time-consuming depending on the scale of optimization problems (including the quantity of continuous and discrete variables and equations involved), and achieving convergence can be challenging.

The process simulators have been applied as standalone (i.e., without coupling with external optimization algorithms) to study LNG optimization: Aspen PLUS (Zhang et al. 2020), Aspen HYSYS (Qyyum et al. 2018a; Castillo et al., 2013). In Zhang et al. (2020), the authors used the "Complex Algorithm" included within Aspen Plus to evaluate four LNG processes encompassing conventional nitrogen expansion and methane expansion processes, with or without ammonia absorption refrigeration machine for pre-cooling. The Complex Algorithm is a "black box" pattern search technique and operates independently of numerical derivatives, and it does not guarantee solution optimality. It may be helpful for simple problems without recycle loops or equality constraints (Javaloyes-Anton et al. 2022; Aspen Plus Technology, 2013). Castillo et al. (2013) analyzed different NG liquefaction process pre-cooling

cycles using Aspen HYSYS process simulation, highlighting the superior efficiency of the three-stage propane pre-cooling cycle among the evaluated cycles. By default, all the process simulators implement the sequential modular approach, which adopts the iteration-and-convergence solving strategy, where the process-units are solved sequentially by eliminating recycle streams (Kang et al. 2022). An advanced option supported by Aspen Plus is the Equation Oriented, permitting the inclusion of certain unsupported models where all the model equations are solved simultaneously via the perturbation layer method. The Perturbation layer method requires a correct definition of import and export variables for calculating derivatives involving the FORTRAN statements. However, implementing rigorous unsupported models within equation-oriented environments increases simulation complexity, introducing challenges in optimization related to variable initialization, potential convergence issues, and extended execution times (Aspen Plus Technology, 2013). In addition, all the process simulators suffer from limitations in the modeling and optimization of multistream heat exchangers (MHEXs), in particular, the lack of any rigorous checks to prevent temperature crossovers and, thus, the possibility that the process simulator could converge to an infeasible design (Vikse et al. 2020; Kamath et al. 2010; Watson et al. 2015). Thus, for large optimization problems, the use of equation-oriented modeling within process simulators is generally discouraged (Aspen Plus Technology, 2013).

Furthermore, mathematical programming (MP) and deterministic optimization methods have been applied to analyze LNG processes (Matovu et al. 2022; Wang et al. 2012; Lee et al. 2022). In contrast to Evolutionary Algorithms, MP and deterministic optimization methods are considered more dependable for optimization tasks. These methods can ensure the optimality of the obtained solutions, whether local or global, by leveraging information regarding the gradients of the functions encompassed within mass, energy, and momentum balances to assess the optimal Karush-Kuhn-Tucker conditions (Edgar et al., 2001). Also, mathematical programming has been applied to address the optimization of Organic Rankine Cycles (Yu et al., 2017; Santos-Rodriguez et al. 2017). Yu et al. (2017) investigated the optimal integration of an ORC into a background process. To this end, a superstructure-based representation of an ORC system embedding several candidate configurations – including turbine bleeding, regeneration, superheating – was implemented in GAMS. Furthermore, a two-stage strategy involving NLP and MILP models was proposed. In the first stage, the optimal configuration and operating conditions of the ORC with heat integration NLP was found by solving a NLP model. In the second stage, the heat exchanger network was found by solving an expanded MILP transshipment model. A case study from the literature was solved to illustrate the effectiveness of the proposed method. As a result, a better integration between

ORC with the process was obtained. Santos-Rodriguez et al. (2017) combined advanced stochastic optimization techniques with first-principles modeling for simultaneous design of working fluids and ORC process under uncertainty. GAMS was used to implement the resulting mathematical models which incorporated detailed physical representations of the system. The proposed optimization approach was able to find novel and non-intuitive working-fluid mixtures while retaining close-to-optimal performance. Several stochastic optimization problems of different complexities and model sizes (up to 80000 variables) were successfully solved by using the local optimization solver CONOPT. The authors emphasized the efficiency of their approach in tackling intricate stochastic optimization problems using detailed models.

Nevertheless, these methods are not very popular in designing and optimizing LNG refrigeration systems because refrigeration processes involve numerous thermodynamic equations that are challenging to resolve within optimization models. Several authors have developed surrogate models to overcome this as simplified representations of process-units and/or to replace the complex calculation of some thermodynamic properties. Surrogate models can be defined from different approaches: statistical regression (Kang et al. 2016), input-output analysis (Keshavarzian et al. 2016), data interpolation, and artificial neural networks (Kesgin et al. 2005). Surrogate models play an important role in creating a link between input data and outputs in cases where the precise relationship between them is unclear. Also, these models hold significant value in reducing the computational complexity involved in solving challenging optimization problems. Applications of surrogate models for the design of natural gas liquefaction processes are found in (Wang et al. 2012, Ali et al., 2018, Santos et al., 2021; Santos et al., 2023). A Mixed-Integer Nonlinear Programming (MINLP) model solved with LINDO, a deterministic optimization algorithm, was applied to minimize the energy consumption of the C3MR cycle (Wang et al. 2012). To simplify the original complexity of MINLP model, the authors used data regression from Aspen Plus to propose simplified thermodynamic functions (including linear, piecewise, or quadratic functions). The solution was obtained from the General Algebraic Modeling System (GAMS), a high-level mathematical programming and optimization modeling tool. A rigorous simulation in Aspen was conducted to validate the results. If the validation process did not align with the expected outcomes, troubleshooting was undertaken in the preceding stages until a validated solution was achieved. In Ali et al. (2018) and Santos et al. (2021), the authors explored the utilization of surrogate-assisted modeling and optimization techniques for Single Mixed Refrigerant (SMR) NG liquefaction processes. In Ali et al. (2018) a surrogate-assisted modeling approach was adopted in combination with EAs (GA or PSO) to identify optimal solutions. Santos et al. (2021) relied on surrogate models, replacing the computationally

intensive rigorous models of Aspen HYSYS, to minimize the shaft power requirement of the PRICO cycle. The authors highlighted the efficacy of surrogate models, specifically kriging, in capturing the essential behavior of first-principles simulations, making them viable alternatives when computational efficiency precedes precise results. Other developments of surrogate models have been applied for Pressure Swing Adsorption (PSA) processes (Li et al. 2020), for a sour water stripping plant (Quirante and Caballero, 2016), for heat exchanger networks (Li et al. 2021), for a hybrid polycrystalline silicon production route (Ramírez-Márquez et al. 2020), for catalytic reforming and isomerization processes (Mencarelli et al. 2020), amine-based CO_2 capture unit (Henao and Maravelias, 2011), for batch distillation separations (Esche et al. 2022), for methanol plant and ammonia reactor series (Forster et al. 2023). Also, surrogate models have been effectively employed in optimizing gas turbine cycles (Kazemian and Gandjalikhan Nassab, 2020), natural gas combined cycles (Rúa et al., 2020; Riboldi et al. 2018), Organic Rankine Cycles (Anteportalatina-García and Martín 2022, Vilasboas et al., 2021, Pagali et al., 2019, Liu et al. 2021). Anteportalatina-García and Martin (2020) successfully introduced a hybrid heuristic-mathematical optimization methodology that simultaneously selects the optimal thermodynamic cycle (a dual pressure Organic Rankine Cycle or an Organic Flash Rankine Cycle), working fluids (benzene or toluene or R227ea), and optimal operating conditions (pressures, temperatures, compositions and flow-rates) for utilizing or reusing low-to-medium temperature waste industrial streams and geothermal brines. To this end, the authors proposed a methodology involving three main stages. In the first stage, a pre-screening task was considered to the aim of reducing the number of candidate fluids and cycles. In the second stage, machine learning was applied in order to obtain surrogate models for the calculation of enthalpy and entropy of the process streams, aiming to bypass the utilization of equations of state. In the third stage, an equation-based optimization approach based on a superstructure-based representation is applied for obtaining the optimal cycle configuration and operating conditions including the selection of the working fluid. Finally, an economic evaluation was carried out by incorporating the trade-off existing between investment and production costs. A case study focused on Spain was employed to present the advantages of the proposed methodology. Vilasboas et al. (2021) investigated Organic Rankine Cycles by proposing surrogate models to substitute the entire optimization model to expedite specific costs and efficiency predictions. This proposal differs from the common practice found in literature, which often involves replacing only a process unit or calculation of some thermodynamic properties. The usage of the proposed surrogate models significantly reduced the processing time, highlighting that the errors associated with

using surrogate models must be analyzed appropriately because they may be prohibitive in some applications.

In contrast to the studies mentioned above, this research addresses the research gap identified in the literature for optimizing LNG processes. It accomplishes this by rigorously computing the thermodynamic properties of process streams within a fully equation-oriented optimization environment using the GAMS platform. To achieve the goal, mathematical models for expanders, compressors, and heat exchangers have been seamlessly integrated with a dynamic-link library (DLL) designed for thermodynamic property estimation based on the Peng-Robinson equation of state. This integration allows for a comprehensive representation of the entire liquefaction process. Another notable contribution is creating a detailed model describing the primary heat exchangers involved in the LNG process. To the best of the authors' knowledge, prior literature has not presented works with the same characteristics and approach as this study, efficiently optimizing the LNG liquefaction processes. This approach incorporates implementing a deterministic mathematical model and utilizing a derivative-based optimization algorithm complemented by extrinsic functions incorporated within DLLs for property estimation.

This study comprises two case studies of significant complexity. In the first case study, pure nitrogen is considered as the refrigerant. In contrast, in the second case study, a mixture of nitrogen and methane and its composition are optimization variables to demonstrate the capability of the model to calculate thermodynamic properties. The primary distinction between pure and mixed refrigerants lies in the temperature profile shape during the gas-liquid phase transition, necessitating an effective solution strategy.

The optimization results derived from the proposed model have been successfully validated through rigorous simulations conducted in a process simulator, Aspen HYSYS, ensuring the accuracy and reliability of the findings. The proposed optimization model and solution strategy offer comprehensive insights into optimizing the liquefaction process from both technical and numerical perspectives. Furthermore, this approach can be applied to any mixed refrigerant-based liquefaction process within the natural gas industry.

2. Process description

A nitrogen dual turbo-expander refrigeration process considered in this study is shown in Figure 1. The process begins with introducing purified natural gas (NG) feed into a series of multistream heat

exchangers (LNG-1, LNG-2, and LNG-3), gradually reducing its temperature. This cooling process occurs in three stages, reaching approximately -160°C following the third heat exchanger (LNG-3).

The high-pressure liquefied natural gas emerging from LNG-3 undergoes a letdown process across VLV-1, resulting in vapor and liquid phases. The vapor-liquid separator (V-1) separates the low-pressure LNG product stream, intended for storage, from the boil-off gas (BOG) stream.

A dual nitrogen turbo-expander cycle is: the high-pressure nitrogen stream (stream #7) is acquired through a three-stage compressor (K-1, K-2, and K-3) equipped with air intercoolers (E-1 and E-2) and an aftercooler (E-3). After passing through LNG-1, the high-pressure nitrogen stream is divided between the warm and cold turbo-expander cycles (EXP-1 and EXP-2). The cooled nitrogen feed for the warm turbo-expander cycle (stream #11) undergoes work expansion in EXP-1, generating the required refrigeration capacity to lower the NG temperature. The remaining portion of the nitrogen stream, serving as the refrigeration fluid for the cold turbo-expander cycle, is further cooled to an intermediate temperature within LNG-2 (stream #14). Subsequently, this cooled nitrogen stream (stream #14) enters the cold turbo-expander cycle, where it experiences work expansion in EXP-2 to achieve pressure levels lower than those of the warm turbo-expander cycle. This controlled pressure reduction is crucial for attaining the minimum temperature required for NG liquefaction. The resulting nitrogen cold stream exiting LNG-3 (stream #16) operates at a pressure level similar to that of the warm expander discharge (stream #12). As a result, streams #12 and #16 are combined to form stream #17. This mixed stream is then subject to reheating within the liquefaction heat exchanger (LNG-2). The reheating process serves to cool the warm and cold nitrogen cycle feed gas streams and to cool and condense the natural gas stream. Finally, the reheated nitrogen gas stream is directed to the first stage of the nitrogen compression system to elevate the pressure of the nitrogen stream.

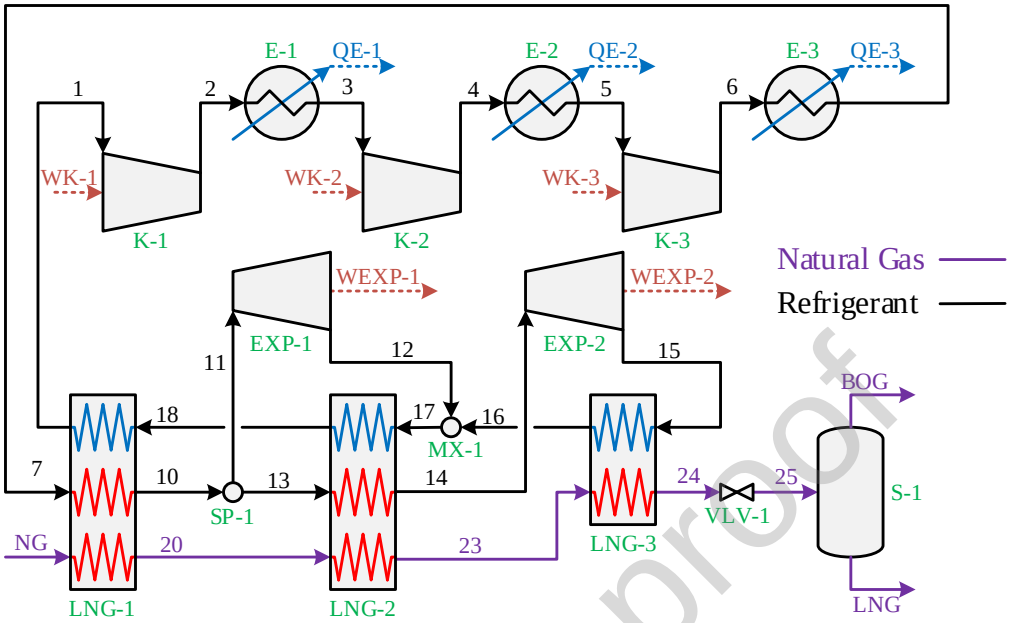

Figure 1. Flow diagram of the evaluated LNG system

Within any LNG process, many trade-offs exist, primarily centered around energy integration within LNG-1, LNG-2, and LNG-3. These trade-offs incorporate the associated heat transfer areas needed and the mass flows and temperature levels of both hot and cold streams. The change in these parameters significantly affects the overall power consumption and the total heat transfer area (and corresponding cost) of all heat exchangers. These trade-offs become notably more conspicuous when the number of cycles in the cascade system increases.

3. Problem statement

The optimization problem consists of minimizing/maximizing an objective function $\mathbf{f}(\mathbf{x})$, which is expressed as:

$$\text{Min/Max } \mathbf{f}(\mathbf{x})$$

subject to:

$-\ \mathbf{hs}(\mathbf{x}) = 0$

$-\ \mathbf{gt}(\mathbf{x}) \leq 0$

– Process design specificacion

where **x** denotes the vector of model variables, the equality constraints, **hs**(**x**), comprise mass and energy balances, correlations for physicochemical properties estimation, and design equations. The variable **gt**(**x**) represents inequality constraints for preventing temperature crossings in heat exchangers and imposing lower and/or upper bounds on critical operating variables. Several objective functions f(**x**) can be considered for optimization, including the minimization of net electrical power ($\dot{W}_{NET}$), total thermal conductance ($U\times A$ value), total heat transfer area, or total annual cost. In this work, two objective functions, $\dot{W}_{NET}$ and $U\times A$ value, are applied. The design specification involves achieving a flow rate of 132 kmol/h of high-pressure LNG at 62.6 bar and 118.15 K, which is then let down across VLV-1, forming two phases (vapor and liquid). The proposed optimization problem aims to obtain the optimal values of temperature, pressure, composition, and flow rate of all process streams for the following output simultaneously:

- Minimum $\dot{W}_{NET}$ value and its optimal distribution between the compressors and expanders.
- Minimum $U\times A$ value and its optimal distribution between the heat exchangers.
- Optimal sizes (sizes of compressors and expanders as well as $U\times A$ values of heat exchangers E-1 to E-3, and LNG-1, LNG-2, and LNG-3).

4. Mathematical model

The mathematical model comprises mass and energy balances for each component within the system, alongside the calculation of heat transfer areas and driving forces. The authors have skillfully incorporated previously established mathematical models developed by their research group for expanders, compressors, and heat exchangers. These models also feature dynamic-link libraries for the estimation of stream properties. This comprehensive integration allows the accurate representation of the LNG process.

Furthermore, the authors have developed specific models tailored to the primary LNG heat exchangers. The readers can find a detailed mathematical model, along with modeling assumptions and numerical values of model parameters, in the "Supplementary Material I" accompanying this article.

4.1. Thermodynamic properties and calculation

The thermodynamic properties of the mixtures involved are estimated using cubic equations of state (CEOS), particularly the Peng-Robinson equation (Yadav et al. 2022). Alternative CEOS with a similar level of accuracy to the Peng-Robinson equation, such as the Soave-Redlich-Kwong equation (Soave, 1993), could also be used.

The Peng-Robinson state equation is

$$P = \frac{R \cdot T}{v - b} - \frac{a(T)}{v^2 + 2 \cdot v \cdot b - b^2} \tag{1}$$

where T and P are the working temperature and pressure, respectively, and R is the universal gas constant. The dependence of the parameter $a(T)$ on the temperature is taken into account by Eq. (2), while the parameter b is calculated from the critical pressure and temperature (P_c and T_c) according to Eq. (3).

$$a(T) = \frac{0.45724 \cdot R^2 \cdot T_c^{\,2}}{P_c}\left[1 + \kappa \cdot \left(1 - \sqrt{T/T_c}\right)\right]^2 \tag{2}$$

$$b = \frac{0.07780 \cdot R \cdot T_c}{P_c} \tag{3}$$

where κ is a characteristic constant of each component, which is calculated in terms of the acentric factor ω as expressed in Eq. (4).

$$\kappa = 0.37464 + 1.54226 \cdot \omega - 0.2699 \cdot \omega^2 \tag{4}$$

Eq. (1) is generally transformed into a cubic equation for the compressibility factor Z, as in Eq. (5), in order to facilitate the mathematical implementation:

$$Z^3 + (B-1) \cdot Z^2 + \left(A - 3 \cdot B^2 - 2 \cdot B\right) Z + \left(B^3 + B^2 - A \cdot B\right) = 0 \tag{5}$$

where

$$A = \frac{a(T) \cdot P}{(R \cdot T)^2} \tag{6}$$

$$B = \frac{b \cdot P}{R \cdot T} \tag{7}$$

For a mixture of components, the variables A and B are calculated using the mixing rules:

$$A = \sum_{i=1}^{c}\sum_{j=1}^{c} x_i \cdot x_j \cdot A_{ij} \tag{8}$$

$$A_{ij} = A_{ji} = \left(1 - k_{ij}\right) \cdot \sqrt{A_i \cdot A_j} \tag{9}$$

$$B = \sum_{i=1}^{n} x_i \cdot B_i \tag{10}$$

where k_{ij} is a binary interaction parameter between components *i* and *j*.

The enthalpy and entropy of the vapor and liquid phases of a refrigerant mixture (or natural gas) are calculated from the departure function forms *(h – h*)* and *(s – s*)*, as expressed in Eq. (11) and Eq. (12), respectively:

$$\frac{(h - h^*)}{R \cdot T} = \frac{A + T \cdot \left(dA/dT\right)}{2 \cdot \sqrt{2} \cdot B} \cdot \ln\left(\frac{Z + B \cdot \left(1 + \sqrt{2}\right)}{Z + B \cdot \left(1 - \sqrt{2}\right)}\right) + \left(Z - 1\right) \tag{11}$$

$$\frac{(s - s^*)}{R} = \frac{2 \cdot A + T \cdot \left(dA/dT\right)}{2 \cdot \sqrt{2} \cdot B} \cdot \ln\left(\frac{Z + B \cdot \left(1 + \sqrt{2}\right)}{Z + B \cdot \left(1 - \sqrt{2}\right)}\right) + \ln\left(Z - B\right) \tag{12}$$

In multicomponent vapor-liquid equilibrium, the fugacity of each component in the liquid and vapor phases must be equal. To calculate the fugacity, the fugacity coefficient for each component *i* is used

$$\ln \phi_i = \left(Z - 1\right) \cdot \frac{B_i}{B} - \ln\left(Z - B\right) + \frac{A}{2 \cdot \sqrt{2} \cdot B}\left(\frac{B_i}{B} - \frac{2\sum_{j=1}^{c} x_j \cdot A_{ij}}{A}\right) \cdot \ln\left\{\frac{Z + B \cdot \left(1 + \sqrt{2}\right)}{Z + B \cdot \left(1 - \sqrt{2}\right)}\right\} \tag{13}$$

Implementing and solving CEOS in deterministic and equation-oriented optimization models is a significant challenge. Two well-defined approaches are typically used. The first methodology (Approach #1) involves considering the complete set of equations related to calculating thermodynamic properties and mass, momentum, and energy balances (Kamath et al., 2010; Dowling and Biegler, 2015). The second option (Approach #2), which is used in this study, proposes the usage of external libraries with user-defined functions to calculate thermodynamic properties (Manassaldi et al., 2019; Bugard et al. 2018).

Approach #1 benefits from being both traditional and relatively straightforward to implement. However, its principal drawback lies in its potential to extend the complexity of the model involving an increased number of variables and equations. Additionally, it poses challenges in finding solutions under certain conditions, such as instances represented by a solitary root of the CEOS, denoting either the liquid or gaseous state. In contrast, Approach #2 offers a distinct advantage by performing effectively across all regions without including equations or supplementary variables. Nonetheless, its primary limitation relies on the implementation software requirement to support embedding user-defined function calls (Bugard et al. 2018).

The software used to implement the proposed model in this research is the General Algebraic Modeling System (GAMS) (GAMS Development Corporation, 2021). The software supports the creation of functions by the user, which are known as extrinsic functions (Manassaldi et al. 2019), and no additional programming effort is required to use them in the current model. Thus, the library of thermodynamic functions developed previously is used to estimate the properties of natural gas and refrigerant (pure N_2 and a mixture of N_2 and CH_4). The functions provided are the enthalpy, entropy, and density of the mixture and the fugacity of each constituent. They all depend on the temperature, pressure, and mole composition of the mixture. For each thermodynamic property, a liquid-phase and a vapor-phase function were created. Applying the method proposed by Deiters and Macias-Salinas (2014), all functions solve the Peng-Robinson cubic polynomial (Eq. (5)). The vapor phase functions use the largest root found, and the liquid phase functions use the smallest root found. Both functions use the unique available root value if only one real root exists. The sequence followed to calculate thermodynamic properties can be found in Supplementary Material II.

The communication between GAMS and the thermodynamic library to calculate the enthalpy of a vapor stream of Approach #2 is illustrated in Figure 2. The GAMS solver sends the input variables (temperature, pressure, and mole fractions), and the library returns the requested property (in this Case, enthalpy) and its corresponding gradient and Hessian matrix (both analytic). In this approach, the model developed to calculate any thermodynamic property (enthalpy in this example) involves nine variables (enthalpy, temperature, pressure, and the six-mole fractions) and one equality equation, while Approach #1 requires 76 variables, 68 equations, and 2 inequalities. Logically, the number of degrees of freedom in both approaches is the same and equal to 8 (76−68=8 for Approach #1 and 9–1=8 for Approach #2), indicating in both cases the direct relationship between a property (e.g., enthalpy) and the 8 main variables of the mixture (temperature, pressure, and the six-mole fractions).

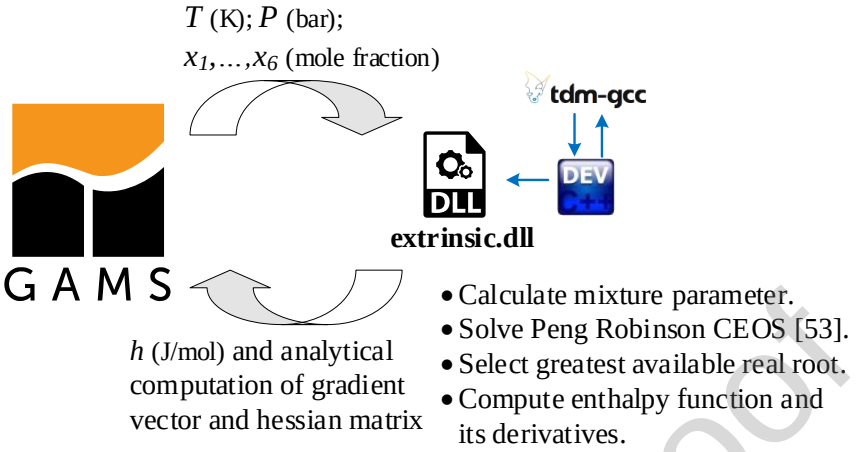

Figure 2. Schematic representation of the interaction between GAMS and dynamic-link library (DLL) for enthalpy calculation of vapor streams in the liquefaction process.

The computation of the thermodynamic properties of each stream (Figure 1) is divided into three groups according to their phase: liquid (L), vapor (V), and L-V. The corresponding functions are applied for the first two cases (L and V). For the third group (L-V), the L-V equilibrium is forced from the equality of the fugacities of each component in each phase. To keep the values within the defined phase, the dew point is calculated for streams #12 and #15.

4.2. Modelling of LNG heat exchangers

As mentioned, the primary challenge when modeling multistream heat exchangers like LNG-1, LNG-2, and LNG-3 is accurately representing the physicochemical and thermodynamic properties of the mixtures involved. This complexity is amplified when considering refrigerants that could be either a single refrigerant (N_2) or a mixed refrigerant (N_2 and CH_4), and natural gas is the fluid to be liquefied considering a mixture of 6 compounds (N_2, CH_4, C_2H_6, C_3H_8, n-C_4H_{10}, i-C_4H_{10}). The nonlinear behavior exhibited by these thermodynamic properties calls for modeling the internal temperature profile within the LNG-1, LNG-2, and LNG-3 exchangers. This is essential to ensure the feasibility of heat transfer and prevent potential temperature overlaps. The mathematical modeling approach for the heat exchanger LNG-2 is shown in Fig. 3.

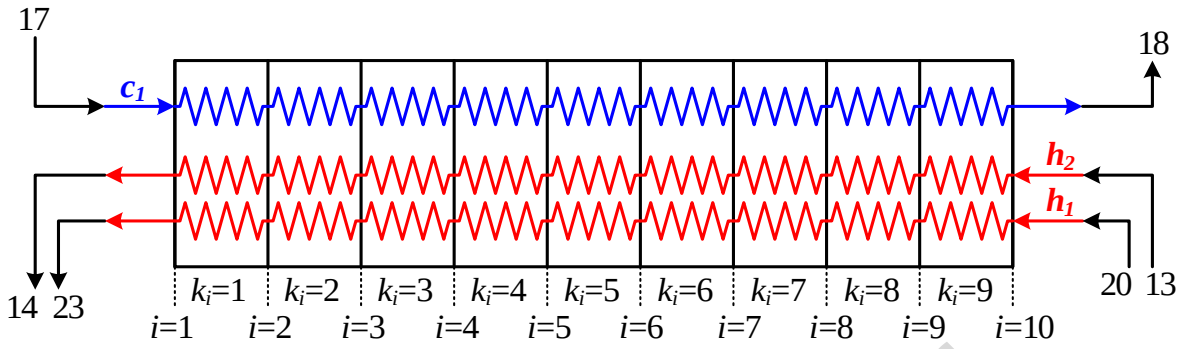

Figure 3. Schematic of the sections and points proposed for the mathematical modeling of LNG-2.

The methodology presented by Pattison and Baldea (2015) guides the implementation of equation-oriented optimization models of multistream heat exchangers. As shown in Fig. 3, there are two hot streams, h_1 (#20) and h_2 (#13), and one cold stream c_1 (#17). The output of the cold stream corresponds to stream #18, while the hot streams h_1 and h_2 outputs correspond to streams #23 and #14, respectively. For simplicity and as a first approximation to verify the model with published results, the hot streams enter and leave the equipment at the same temperature, i.e., $T_{13} = T_{20}$ and $T_{14} = T_{23}$.

The hot streams h_1 and h_2 form a hot composite stream, while the cold stream c_1 represents the cold composite stream. To correctly describe the behavior of the temperature profile, heat transfer, driving forces, and heat transfer area in LNG-2, it is proposed to divide the heat exchanger into 10 points indicated as i and 9 sections as k_i (Fig. 3).

At the ends of the heat exchangers, the involved hot and cold streams must be coupled with the hot and cold composite currents, respectively. The cold streams enter through point i=1 while the hot streams enter through point i=10. Therefore, the temperature of the cold composite stream at point i=1 must be equal to the temperature of stream #17 (Eq. (14)). The same applied to the hot composite stream in the first point (Eq. (15) and Eq. (16)). While Eqs. (17)–(19) apply to both streams in the last point (i=10).

$$T_c^i = T_{17} \qquad i=1 \qquad (14)$$

$$T_h^i = T_{14} \qquad i=1 \qquad (15)$$

$$T_h^i = T_{23} \qquad i=1 \qquad (16)$$

$$T_c^i = T_{18} \qquad i=10 \qquad (17)$$

$$T_h^i = T_{13} \qquad i=10 \qquad (18)$$

$$T_h^i = T_{20} \qquad i=10 \tag{19}$$

The following equations (20–25) are used for the pressure calculation of each stream inside the heat exchangers:

$$P_{c1}^i = P_{17} \qquad i=1 \tag{20}$$

$$P_{h1}^i = P_{23} \qquad i=10 \tag{21}$$

$$P_{h2}^i = P_{14} \qquad i=10 \tag{22}$$

$$P_{c1}^{i+1} = P_{c1}^i - \frac{\Delta P_{LNG}}{9} \qquad i=1,2,\ldots,9 \tag{23}$$

$$P_{h1}^i = P_{h1}^{i+1} - \frac{\Delta P_{LNG}}{9} \qquad i=1,2,\ldots,9 \tag{24}$$

$$P_{h2}^i = P_{h2}^{i+1} - \frac{\Delta P_{LNG}}{9} \qquad i=1,2,\ldots,9 \tag{25}$$

Eq. (26) and Eq. (27) are proposed to calculate the total heat load (mH) of stream h_1 and h_2, respectively, in each of the defined points. In each point, the enthalpy value is calculated using the Peng-Robinson equation. The enthalpy values calculated in point i=1 (i.e., h_{23} and h_{14}) are taken as reference values, so the energy content of these streams in this point is zero. Consequently, the total energy calculated in point i=10 is the total energy supply. The convenience of using point i=1 as a reference is that it allows handling positive energy content values and, thus, effortlessly creates the hot and cold composite curves on the temperature-enthalpy diagram.

$$mH_{h1}^i = m_{23} \cdot \left(H_{h1}^i - h_{23} \right) \qquad i=1,2,\ldots,10 \tag{26}$$

$$mH_{h2}^i = m_{14} \cdot \left(H_{h2}^i - h_{14} \right) \qquad i=1,2,\ldots,10 \tag{27}$$

Similarly, Eq. (28) is used to calculate the energy content of the cold stream, again using point i=1 (cold stream inlet) as the reference.

$$mH_{c1}^i = m_{17} \cdot \left(H_{c1}^i - h_{17} \right) \qquad i=1,2,\ldots,10 \tag{28}$$

Thus, the energy balance for each section and the heat load ($q_{LNG-2}^{z_i}$) are expressed by Eq. (29) and Eq. (30), respectively:

$$q_{LNG-2}^{k_i} = \left(mH_{h1}^{i+1} - mH_{h1}^i \right) + \left(mH_{h2}^{i+1} - mH_{h2}^i \right) \qquad i=1,2,\ldots,9 \tag{29}$$

$$q_{LNG-2}^{k_i} = mH_{c1}^{i+1} - mH_{c1}^i \qquad i=1,2,\ldots,9 \tag{30}$$

For mathematical modeling, it is assumed that the heat exchanged in all sections of the heat exchanger is the same; therefore, the entire heat exchanged is discretized into sections with equally-spaced enthalpy (q_{LNG-2}) from its inlet to outlet enthalpy values, as shown in Fig. 4 and expressed in Eq. (31). Then, the composite curves are obtained summing up the relevant enthalpy changes of hot and cold streams at a given temperature.

$$q_{LNG-2}^{k_i} = q_{LNG-2}^{k_{i+1}} \qquad i = 1,2,\ldots,8 \tag{31}$$

Eq. (32) guarantees the feasibility of heat exchange by imposing that the temperature of the hot composite stream T_h^i in each of the points must be greater than or equal to the temperature of the cold composite stream T_c^i plus a minimum temperature difference $\Delta T_{\min}$.

$$T_h^i \geq T_c^i + \Delta T_{\min} \qquad i = 1,2,\ldots,10 \tag{32}$$

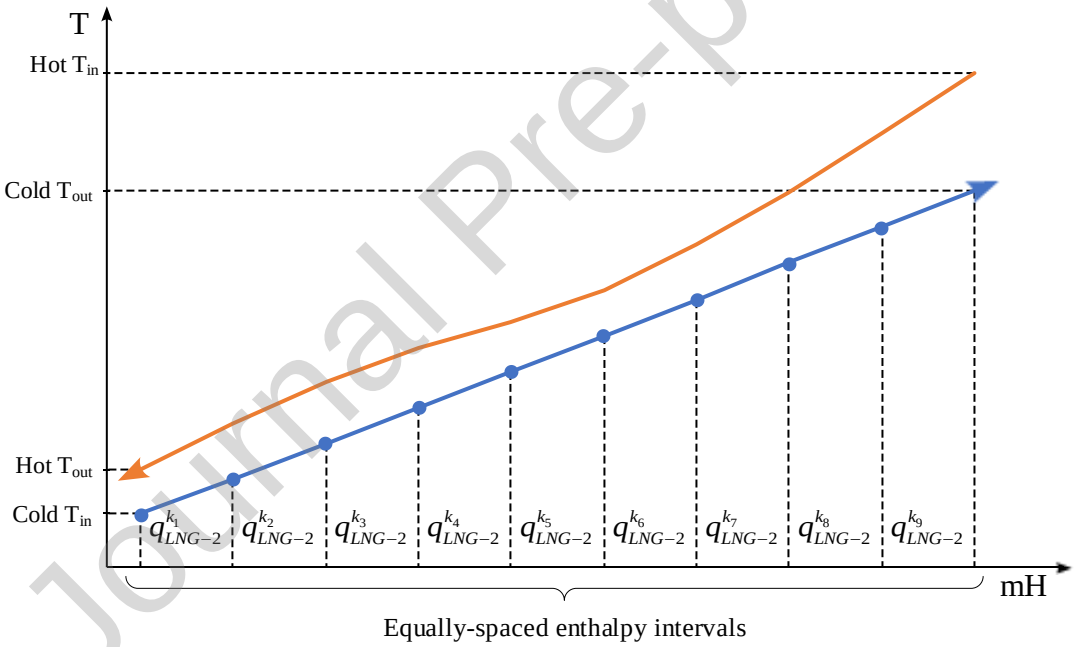

Figure 4. Temperature-enthalpy rate diagram of the equally-spaced enthalpy sections considered for the mathematical modeling of LNG-2.

Finally, Eqs. (33)–(35) establish the relationship between the enthalpy of every stream in each point with the temperature (*T*), pressure (*P*), and composition (*x*) of the composite stream. For this purpose, the authors have used previously developed extrinsic functions (Manassaldi et al. 2019).

$$H_{h1}^i = f_{vap}\left(T_h^i, P_{h1}^i, x_{23}\right) \qquad i = 1,2,\ldots,10 \tag{33}$$

$$H_{h2}^{i} = f_{vap}\left(T_{h}^{i}, P_{h2}^{i}, x_{14}\right) \qquad i = 1,2,\ldots,10 \tag{34}$$

$$H_{c1}^{i} = f_{vap}\left(T_{c}^{i}, P_{c1}^{i}, x_{17}\right) \qquad i = 1,2,\ldots,10 \tag{35}$$

Finally, Eq. (36) calculates the total value $U \times A$ required by the LNG-2 heat exchanger:

$$\left(UA\right)_{LNG-2} = \sum_{i=1}^{9} \frac{q_{LNG-2}^{k_i}}{LMTD_{LNG-2}^{k_i}} \tag{36}$$

where q_{LNG-2} is the heat exchanged in each of the exchanger sections and $LMTD_{LNG-2}^{i}$ represents the driving force in the associated section k_i calculated by the logarithmic mean approximation proposed by Chen (2019) and expressed as:

$$\Delta T_{LNG-2}^{k_i} = \sqrt[3]{0.5 \cdot \left(T_h^i - T_c^i\right) \cdot \left(T_h^{i+1} - T_c^{i+1}\right) \cdot \left(\left(T_h^i - T_c^i\right) + \left(T_h^{i+1} - T_c^{i+1}\right)\right)} \qquad i = 1,2,\ldots,9 \tag{37}$$

The model size increases significantly with the addition of the internal modeling of the multistream heat exchangers. The greater the number of heat exchanger sections, the better the capture of the behavior of the thermodynamic properties of the streams. Similarly, Eqs. (1)–(37) are extended to model the LNG-1 and LNG-3 heat exchangers.

The complete NLP mathematical model contains 507 variables and 612 equality and inequality constraints. The GAMS (v.24.8.5) is used to implement the model. The model is solved using the CONOPT 3 solver (Drud, 1996), a local optimizer based on the generalized reduced gradient (GRG) algorithm.

5. Solution strategy

To ensure the convergence of the model, given its highly nonlinear nature characterized by the presence of bilinear terms and logarithmic functions, a preprocessing phase has been created to initialize the model effectively. The objective is to find an initial solution that is either entirely feasible or, at the very least, exhibits minimal infeasibilities. As illustrated in Fig. 5, the preprocessing phase entails solving a series of three models sequentially, denoted as Model-1, Model-2, and Model-3, as the process unfolds.

The core principle underpinning this preprocessing phase is that the optimal solution derived for Model "*j*" is automatically used as the initialization for the subsequent solution of Model "*j*+1," until the final rigorous and comprehensive model is resolved. This phase capitalizes on the fact that an optimal solution,

or at the very least a quasi-feasible solution (meaning it contains only a few infeasibilities), serves as a robust starting point for addressing a larger model.

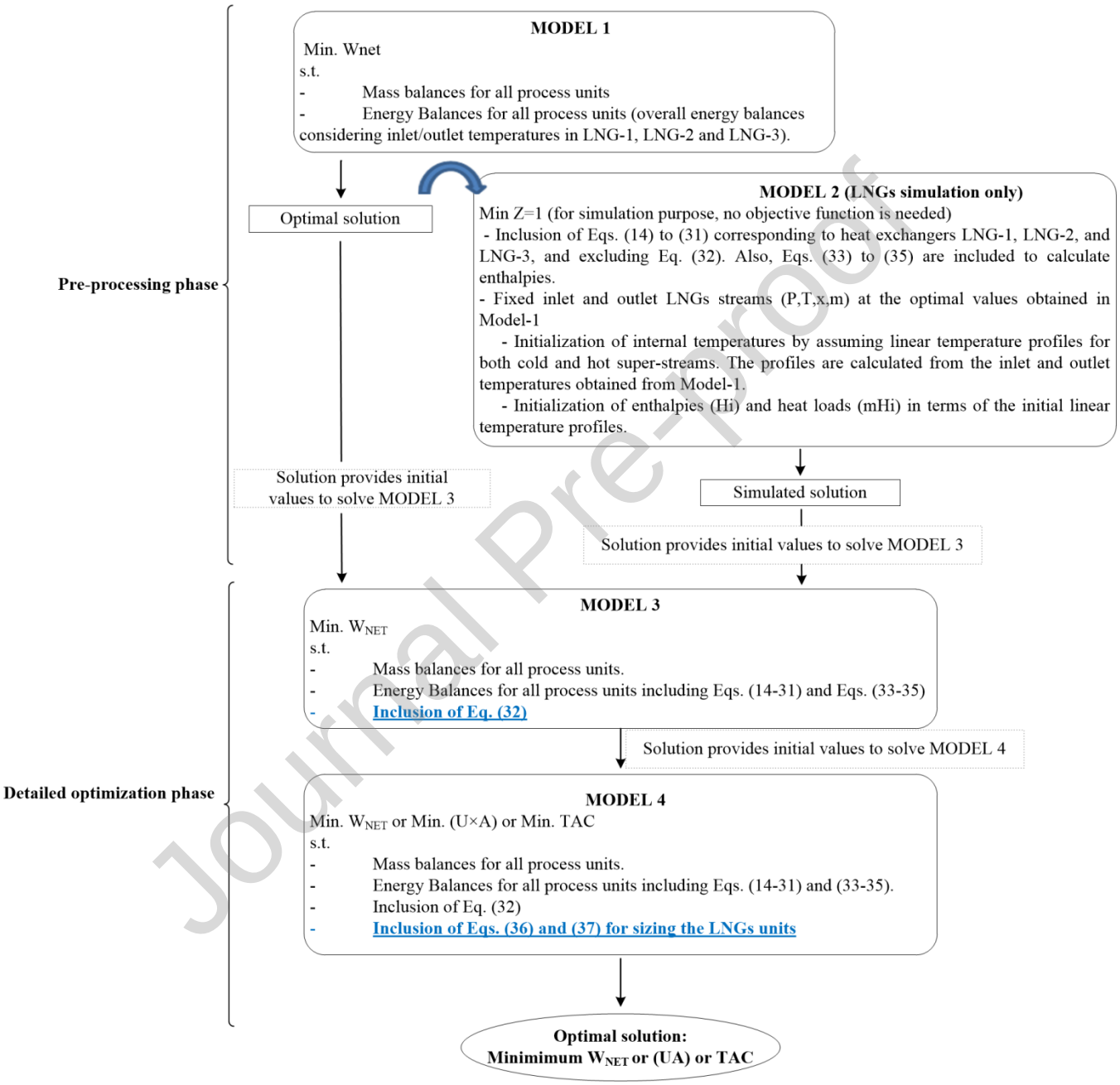

Figure 5. Steps involved in the proposed solution strategy.

As a first step, it is proposed to solve Model-1, which corresponds to the simplest and most reduced model since it includes only the material and energy balances and the calculation of the thermodynamic properties of all process streams. However, in this model, the energy balances in the heat exchangers LNG-1, LNG-2, and LNG-3 are calculated using only the energy values at the hot and cold ends, thus avoiding temperature crossings at these ends ($T_{10}>T_{18}+\Delta T_{min}$ and $T_{7}>T_{1}+\Delta T_{min}$ in LNG-1, $T_{13}>T_{18}+\Delta T_{min}$ and $T_{14}>T_{17}+\Delta T_{min}$ in LNG-2, and $T_{23}>T_{16}+\Delta T_{min}$ and $T_{24}>T_{15}+\Delta T_{min}$ in LNG-3). Model-1 offers the advantage that, despite its inherently nonlinear character, its convergence is not overly reliant on the initial variable values. It exhibits convergence irrespective of variations in parameter values. Nonetheless, should issues with convergence arise, an ideal thermodynamic model stands as a potential solution for initialization. Given that the thermodynamic model is incorporated via an external function, replacing the Peng-Robinson model with an ideal one during this preprocessing step is straightforward. Subsequently, in the following step, the Peng-Robinson model can be re-executed and resolved using the solution from the ideal model as the starting point.

It is important to note that this approach does not include the (internal) segments of the heat exchangers and, consequently, the internal temperature profiles. As a result, it is not feasible to impose inequality constraints aimed at preventing internal temperature overlaps within the heat exchangers. However, it is worth emphasizing that the last model in this phase (Model-3) ensures the feasibility of internal heat exchanges within LNG-1, LNG-2, and LNG-3.

The solution obtained from Model-1 successfully fulfills the mass and energy balances. However, there may still be internal temperature crossovers within any (or all) of the multistream heat exchangers, namely LNG-1, LNG-2, and LNG-3. This is because the model does not yet account for internal temperature profiles. To take advantage of the outcomes of Model-1, the authors introduce a subsequent Model-2. In this model, only the three multistream heat exchangers (LNG-1, LNG-2, and LNG-3) are solved in simulation mode, with fixed inlets and outlets LNGs streams (P, T, x and m) at the optimal values obtained from Model-1. The primary purpose of Model-2 is to simulate the internal temperature profile corresponding to the solution of Model-1, so Eq. (32) is omitted since ensuring the minimum temperature difference cannot be guaranteed at this stage. Consequently, Model-2 encompasses the energy balance for each heat exchanger section and calculates the enthalpy at each point.

As an initialization strategy for Model-2, the temperatures using a linear temperature profile of the composite streams should be computed first. This profile is developed using the optimal temperatures obtained at the ends of the heat exchangers from Model-1. These initial temperature values are then

automatically used to initialize the corresponding enthalpies and, subsequently, the remaining variables (e.g., mH and qLNG). The reasoning behind this initialization approach is that thermodynamic properties are inherently explicit in the enthalpy. As a result, establishing a linear temperature profile and calculating the enthalpies constitute a straightforward sequential process with no intermediate iterations. Although this initialization point (temperature linear profile) does not exactly correspond to an initially feasible solution for Model-2, it serves as an easy-to-generate initialization point with very few infeasibilities in the energy balances. It should be mentioned that these infeasibilities do not hinder the convergence of this model, as discussed below in the presentation of the case studies.

The combination of solutions from Model-1 and Model-2 results in a "potential" feasible solution for the final model. This combined solution satisfies all model constraints except for Eq. (32), which ensures heat exchange feasibility and has not been incorporated in any prior model. For this reason, Eq. (32) may or may not be satisfied at all points within the heat exchanger in Model-3. Consequently, the third phase of the preprocessing includes the resolution of the comprehensive Model-3, introducing Eq. (32) to secure heat exchange feasibility. It is important to note that Model-3 can solve the entire process simultaneously with the internal temperature profiles of the multistream heat exchangers. If Model-2 satisfies Eq. (32) at all points, the new solution (Model-3) will mirror the current one (Model-1+Model-2). But if Model-2 does not satisfy Eq. (32) at all points, then Model-3 can modify the process variables to satisfy it, and the new solution (Model-3) will be slightly different from the current one. In this last situation, since it is a minimization problem, the new value of the objective function will be slightly higher than Model-1, $W_{NET(Model\text{-}3)} > W_{NET(Model\text{-}3)}$.

Lastly, the authors propose addressing Model-4 as the final detailed model. Compared to Model-3, Model-4 incorporates all equations relevant to the computation of the driving force – logarithmic mean temperature difference (LMTD) and U×A values in each section of the heat exchangers LNG-1, LNG-2, and LNG-3. The primary advantage of introducing Model-4 in the latter preprocessing stage is that all the newly introduced optimization variables (LMTD and $U{\times}A$ values) can be initialized based on the optimal values of flows, temperatures, and enthalpies obtained from Model-3. Regardless of the objective function considered in Model-4, the optimal solution of Model-3 serves as an initial feasible point for solving Model-4. For instance, if Model-4 retains the same objective function as Model-3 (minimization of $\dot{W}_{NET}$), the optimal solution will be identical for both optimization problems. The distinction lies in the computation of the corresponding optimal $U{\times}A$ values in Model-4. On the contrary, if Model-4 adopts a different objective function than Model-3 (e.g., minimization of $U{\times}A$ value or cost reduction), the solution

from Model-3, coupled with its associated initial values of U×A and LMTD, will serve as a genuinely feasible starting point for Model-4. This ensures that all model constraints (inequalities and equalities) are satisfied, thus guaranteeing the convergence of the entire model.

6. Results and Discussions

Three case studies are presented to verify the proposed model and the obtained optimization results. An optimal solution obtained using the Aspen HYSYS/GA algorithm reported in (Moein et al. 2015) is used as a base case to verify the accuracy of the model (case study I), and to compare the obtained optimal solutions (case studies II and III). The data set listed in Table 1 was assumed for all cases, which are solved on a 3.3 GHz AMD six-core processor with 4 GB of RAM.

Table 1. Numerical values of the parameters used in the case studies (Moein et al. 2015).

Parameter and unit	Value
Isentropic compressor efficiency (%)	75
Minimum temperature approach, ΔT_{min} (K)	2
Pressure drop in LNG heat exchangers (bar)	0.1
Pressure drop in air coolers (bar)	0.2
Flow rate of natural gas, $\dot{m}_{NG}$ (kmol/h)	132
Pressure of natural gas entering cold box, P_{NG} (bar)	62.9
Temperature of hot stream at cold box inlet, T_{NG} (K)	313.15
Temperature of natural gas at cold box outlet, T_{24} (K)	118.15
Natural gas valve discharge pressure, P_{25} (bar)	1.01325
Composition of natural gas (mole%)	
N_2	0.9
CH_4	94
C_2H_6	3.1
C_3H_8	1.3
n-C_4H_{10}	0.4
i-C_4H_{10}	0.3

6.1. Case study I: Verification of the model

The model accuracy was validated by comparing the values with the ones reported in (Moein et al. 2015). For the verification, the case study was simulated by fixing several optimization variables in the proposed model with the same values as in (Moein et al. 2015) to maintain the degrees of freedom. Table 2 lists the variables fixed for the verification process and their corresponding numerical values. Table 3 provides a comparison of the output values of the main model variables with the values explicitly reported in (Moein et al. 2015).

Table 2. Optimization variables with their numerical values fixed for model verification.

Parameter and unit	Value
T_1 (K)	311.15
T_{20} (K)	268.11
T_{23} (K)	178.34
P_2 (bar)	9.97
P_4 (bar)	20.06
P_6 (bar)	40.03
P_{15} (bar)	4.54

As shown in Table 3, the output values of the main process variables agree with the values reported in (Moein et al. 2015). The differences in the obtained numerical values are less than 0.35%.
The values of pressure, temperature, and flow rate of all streams are given in Table 4. The $U \times A$ values corresponding to all heat exchangers are presented in Table 5.

The proposed mathematical model was used as a "simulator" for verification purposes, i.e., no degrees of freedom were considered in this Case. This contrasts with the following case studies, where the model is used as an "optimizer".

Table 3. Comparison of the main process variables used for model verification**.**

	Base case (Moein et al. 2015)	This work	Diff (%)
Net required work ($\dot{W}_{NET}$, kW)	1402.9	1398.4	(-) 0.32
Flow rate of nitrogen ($\dot{m}_{ref}$, kmol/h)	0.2142	0.2147	(+) 0.22

Table 4. Simulated values obtained for temperature, pressure, and flowrates corresponding to the base case.

Stream	T (K)	P (bar)	$\dot{m}$ (kmol/s)
#1	311.1	4.238	0.2147
#2	424.3	9.969	0.2147
#3	311.1	9.769	0.2147
#4	404.7	20.050	0.2147
#5	311.1	19.850	0.2147
#6	402.1	40.030	0.2147
#7	313.1	39.830	0.2147
#10	268.1	39.730	0.2147
#11	268.1	39.730	0.1500

#12	168.6	4.438	0.1500
#13	268.1	39.730	0.0646
#14	178.3	39.63	0.0646
#15	105.1	4.538	0.0646
#16	176.3	4.438	0.0646
#17	170.9	4.438	0.2147
#18	250.7	4.338	0.2147
NG	313.1	62.900	0.0367
#20	268.1	62.800	0.0367
#23	178.3	62.700	0.0367
#24	118.1	62.600	0.0367
#25	111.0	1.013	0.0367

Table 5. Results of the heat exchangers for the base case.

Heat exchanger	$U \times A$ (kW/K)
E-1	15.75
E-2	14.78
E-3	13.84
LNG-1	54.54
LNG-2	80.33
LNG-3	18.45
Total	197.72

6.2. Optimization results

6.2.1 Case study II: Minimization of total net electrical power consumption

The proposed mathematical model for the minimization of the net electrical power ($\dot{W}_{NET}$) is solved by "relaxing" all the variable values that were mentionned in Table 2 for model verification (case study I). These variables are now considered as optimization variables. In this case study, the refrigerant is pure N_2. The optimal solution obtained is referred to as OptimDes I.

The optimization results (OptimDes I) are compared in Tables 6 through 10 with those obtained for the base case, as presented in (Moein et al. 2015). The base case solution was obtained using a genetic algorithm combined with Aspen HYSYS and presented as the best solution found, considering pure N_2 as the refrigerant.

In Table 6, the net electrical power in OptimDes I is presented. It decreased from 1398 kW to 1277 kW, which means 8.7% compared to the base case. This reduction was mainly due to the decrease in power

consumption of all compressors, while the electrical power generated by the expanders remained almost constant (Table 7). The most significant reduction in electrical power is observed for Compressor K-1, followed by K-3 and K-2. However, the decrease in total power resulted in a 40% increase in the total $U \times A$ value (Table 8). As observed when comparing the values in Table 8, there is a greater energy integration between the hot and cold streams in the LNG-1, LNG-2, and LNG-3 heat exchangers due to the change in operating conditions (Table 9), which necessarily requires higher total $U \times A$ values in these units (Table 8).

Table 6. Comparison of the net electrical power, thermal conductance, refrigerant flow rate, and minimum temperature difference between the optimal solution and base case (N_2 as refrigerant only).

	Base Case Optimal solution (ASPEN HYSYS + Genetic Algorithm)	This work OptimDes I (Derivate-based Optimization Algorithm)	Diff. (%)
$\dot{W}_{NET}$ (kW)	1398	1277	(-) 8.7
$U \times A$ (kW/K)	197	277	(+) 40.3
$\dot{m}_{ref}$ (kmol/s)	0.22	0.25	(+) 17.6
$\Delta Tmin$ (K)	2.0	2.0#	

Optimal value reached the lower bound

Table 7. Comparison of the electrical power required for the compressor and generated by expanders between the optimal solution and base case (pure N_2 as refrigerant).

		Base Case Optimal solution (ASPEN HYSYS+Genetic Algorithm)	This work, OptimDes I (Derivate-based Optimization Algorithm)	Diff. (%)
Compressor	K-1	716.9	641.6	(-) 10.5
	K-2	591.0	578.1	(-) 2.2
	K-3	574.8	539.4	(-) 6.2
		1882.7	1759.1	(-) 6.6
Expander	EXP-1	389.1	384.8	(-) 1.1
	EXP-2	95.3	97.1	(+) 1.8
		484.4	481.9	(-) 0.5

Table 8. Comparison of the total heat loads, thermal conductance, and LMTD between the optimal solution and base case (pure N_2 as refrigerant).

	Base Case Optimal solution (ASPEN HYSYS + Genetic Algorithm)	This work OptimDes I (Derivate-based Optimization Algorithm)	Diff. (%)
LNG-1	380.1	494.0	(+) 30
LNG-2	500.9	498.5	(-) 0.5
LNG-3	137.3	141.7	(+) 3.2
Total	1018.3	1134.2	(+) 11.4
E-1	725.0	651.9	(-) 10.1

$\dot{Q}$ (kW)	E-2	605.5	595.1	(-) 1.7
	E-3	588.5	550.9	(-) 6.4
	Total	1919.0	1797.9	(-) 6.3
	Total	2937.3	2932.1	(-) 0.2
	LNG-1	54.5	71.4	(+) 31.1
	LNG-2	80.3	119.3	(+) 48.6
	LNG-3	18.4	38.7	(+) 110.1
	Total	153.1	229.4	(+) 49.8
$U \times A$ (kW/K)	E-1	15.7	16.7	(+) 6.1
	E-2	14.7	16.2	(+) 9.7
	E-3	13.8	14.8	(+) 6.9
	Total	44.2	47.7	(+) 7.6
	Total	197.3	277.1	(+) 40.3
	LNG-1	6.9	6.9	(-) 0.9
	LNG-2	6.2	4.1	(-) 33
LMTD (K)	LNG-3	7.4	3.6	(-) 50.9
	E-1	46.0	39.0	(-) 15.2
	E-2	40.9	36.6	(-) 10.4
	E-3	42.5	37.2	(-) 12.5

Table 9. Optimal values of pressure, temperature, and flowrates obtained for the base case and OptimDes I (N_2 as refrigerant only)

	Base Case ASPEN HYSYS + Genetic Algorithm Optimal solution			This work Derivate-based optimization algorithm OptimDes I		
	T (K)	P (bar)	$\dot{m}$ (kmol/s)	T (K)	P (bar)	$\dot{m}$ (kmol/s)
1	311.2	4.238	0.2147	311.2	6.462	0.2526
2	424.4	9.969	0.2147	397.5	12.616	0.2526
3	311.2	9.769	0.2147	311.2	12.416	0.2526
4	404.7	20.059	0.2147	389.1	22.809	0.2526
5	311.2	19.859	0.2147	311.2	22.609	0.2526
6	402.1	40.033	0.2147	383.9	40.000	0.2526
7	313.2	39.833	0.2147	313.2	39.800	0.2526
10	268.1	39.733	0.2147	262.0	39.700	0.2526
11	268.1	39.733	0.1501	262.0	39.700	0.1773
12	168.6	4.438	0.1501	177.9	6.662	0.1773
13	268.1	39.733	0.0646	262.0	39.700	0.0753
14	178.3	39.633	0.0646	179.9	39.600	0.0753
15	105.2	4.5383	0.0646	116.2	6.762	0.0753
16	176.3	4.4383	0.0646	177.9	6.662	0.0753
17	171.0	4.4383	0.2147	177.9	6.662	0.2526
18	250.8	4.3383	0.2147	244.8	6.562	0.2526
NG	313.2	62.900	0.0367	313.2	62.900	0.0367
20	268.1	62.800	0.0367	262.0	62.800	0.0367
23	178.3	62.700	0.0367	179.9	62.700	0.0367

24	118.2	62.600	0.0367	118.2	62.600	0.0367
25	111.1	1.0133	0.0367	111.1	1.013	0.0367

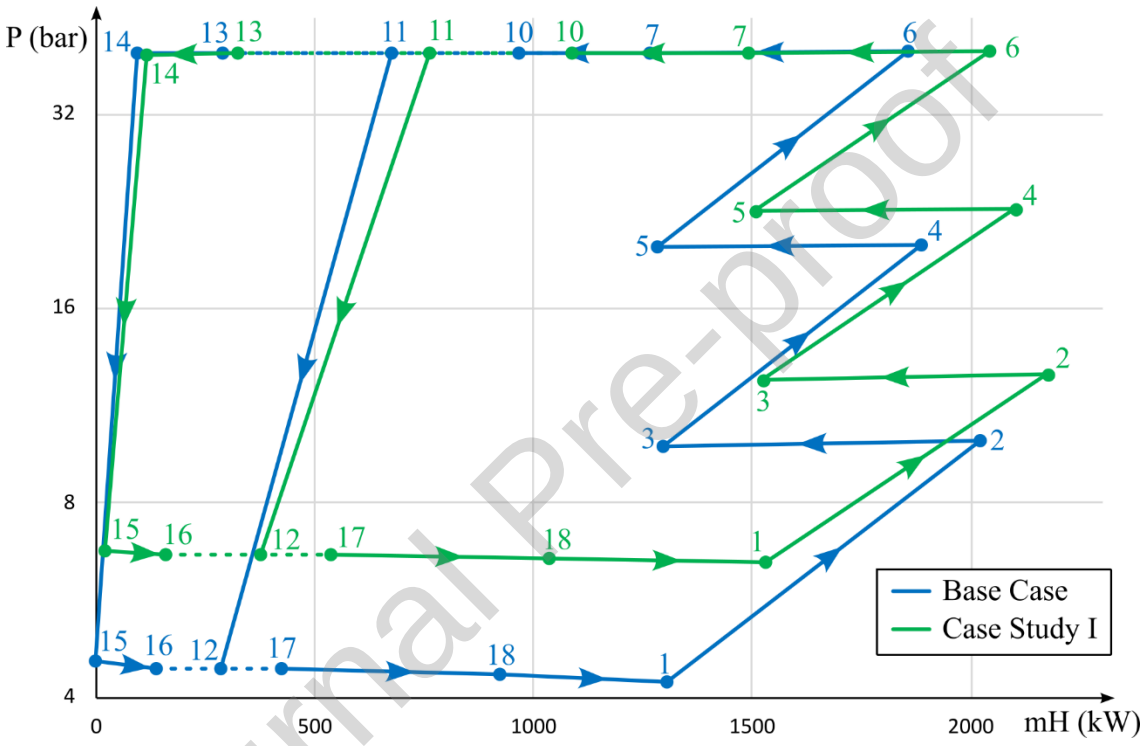

Figure 6. Comparison of the thermodynamic cycle on a pressure-enthalpy diagram.

The optimal pressure values at the inlet of the compressors obtained in OptimDes I are higher compared to the base case, as presented in Table 9 and Figure 6. The difference between the inlet and outlet pressures in K-1 and the refrigerant flow rate obtained in this work is slightly higher than in the base case (6.15 bar vs. 5.73 bar and 0.2526 kmol/s vs. 0.2147 kmol/s), the temperature difference is much lower (86.3 K vs. 113.2 K), but with a more significant influence on the enthalpy difference (2540.35 J/mol vs. 3339.49 J/mol), resulting in a lower electrical power requirement compared to the base case (641.6 kW vs. 716.9 kW).

According to Table 8, the LNG-1 heat exchanger increases the heat load by 113 kW compared to the base case (from 380.1 kW to 494.0 kW). Since the optimal value of the “average” LMTD is the same in both

cases (6.9 K), a corresponding $U\times A$ value must increase by 17 kW/K (from 54.5 kW/K to 71.4 kW/K). However, the increase of the $U\times A$ values in LNG-2 and LNG-3 is due to the decrease of the LMTD in both cases since the heat loads are almost the same. For example, the difference in heat load in LNG-3 is only 4.4 kW (141.7 kW obtained in this work and 137.3 kW for the base case), but with a significant difference in driving forces, with 3.6 K in this work compared to 7.4 K for the base case). This implies an increase in the U×A total value of 20.3 kW/K (from 18.4 kW/K to 38.7 kW/K). The same behavior between heat loads, driving forces, and $U\times A$ values is observed for LNG-1.

Finally, it is interesting to show the optimal distribution of the transferred heat, LMTD, $U\times A$ values, and temperature differences within the heat exchangers LNG-1, LNG-2, and LNG-3 (Table 10 and Fig. 7).

Table 10. Optimal distributions of q_{LNG}, *LMTD*, $U\times A$ value, and ΔT obtained in OptimDes I

		q_{LNG} at section k_i		*LMTD* at section k_i		($U\times A$) value at section k_i		ΔT at point i		
		OptimDes I	Base case	OptimDes I	Base case	OptimDes I	Base case		OptimDes I	Base case
LNG-1	$k_{i=1}$	123.5	95.0	3.5	3.5	35.3	27.0	i=1	2.0#	2.0#
	$k_{i=2}$	123.5	95.0	7.3	7.4	16.9	12.9	i=2	5.6	5.7
	$k_{i=3}$	123.5	95.0	11.1	11.3	11.1	8.4	i=3	9.3	9.4
	$k_{i=4}$	123.5	95.0	15.1	15.2	8.2	6.2	i=4	13.2	13.3
								i=5	17.2	17.3
LNG-2	$k_{i=1}$	55.4	55.7	14.4	14.5	3.8	3.8	i=1	17.2	17.3
	$k_{i=2}$	55.4	55.7	9.4	9.6	5.9	5.8	i=2	11.9	12.1
	$k_{i=3}$	55.4	55.7	5.3	5.7	10.4	9.8	i=3	7.3	7.5
	$k_{i=4}$	55.4	55.7	2.8	3.4	19.9	16.2	i=4	3.7	4.2
	$k_{i=5}$	55.4	55.7	2.4	3.6	22.9	15.6	i=5	2.0#	2.8
	$k_{i=6}$	55.4	55.7	3.8	5.9	14.6	9.4	i=6	2.9	4.5
	$k_{i=7}$	55.4	55.7	5.1	8.4	11.0	6.6	i=7	4.9	7.7
	$k_{i=8}$	55.4	55.7	4.6	9.0	11.9	6.2	i=8	5.3	9.2
	$k_{i=9}$	55.4	55.7	2.9	8.1	19.0	6.9	i=9	4.1	8.8
								i=10	2.0#	7.4
LNG-3	$k_{i=1}$	35.4	34.3	3.1	4.0	11.6	8.7	i=1	2.0#	2.0#
	$k_{i=2}$	35.4	34.3	4.7	8.5	7.5	4.0	i=2	4.4	7.0
	$k_{i=3}$	35.4	34.3	4.6	11.3	7.7	3.1	i=3	5.1	10.3
	$k_{i=4}$	35.4	34.3	3.0	12.6	12.0	2.7	i=4	4.2	12.3
								i=5	2.0#	13.0
Total		1134.3	1018.4			229.7	153.3			

Optimal value reached the lower bound

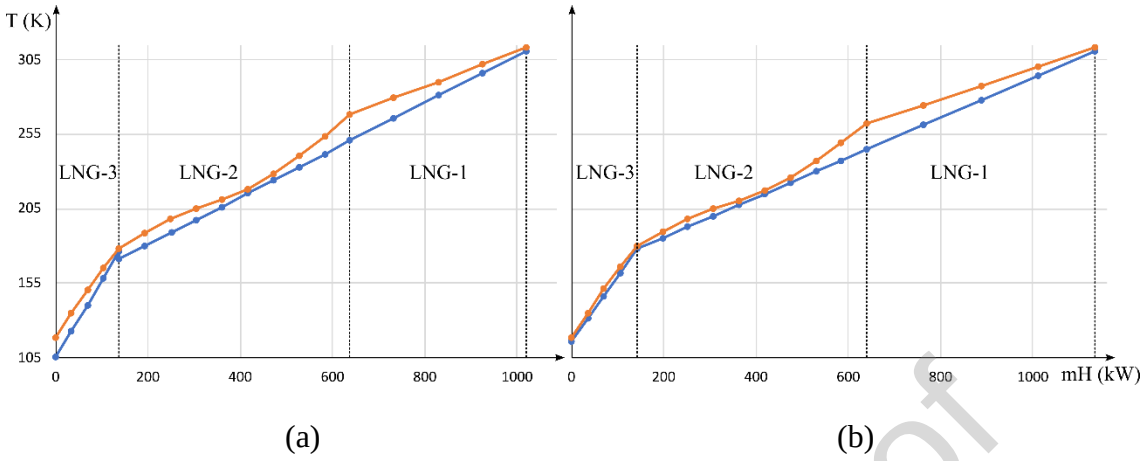

(a) (b)

Figure 7. temperature-enthalpy rate diagrams: (a) base case (simulation), (b) case study I (optimization).

As shown in Fig. 7, the hot stream profiles of exchangers LNG-1 and LNG-3 appear to be linear in both simulated and optimized solutions, while LNG-2 appears to behave differently. Therefore, it can be predicted that LNG-2 is the heat exchanger with the most difficulty in converging. Convergence is improved by increasing the number of points used to model the exchangers. In the cases solved in this work it was enough to consider 10 points (9 sections) for LNG-2, and 5 points (4 sections) for both LNG-1 and LNG-3. It is worth noting that if the model encounters convergence issues due to other design specifications, the number of points should be increased, which is a simple task since the model considers this number as a parameter, and all equations are implemented as a function of this parameter.

6.2.2 Case study III: Comparison of optimal solutions for single and mixed refrigerants by minimizing the total $U \times A$ value

The updated optimization problem investigates whether using a refrigerant blend would be advantageous from an optimization perspective. Thus, the new case study introduces the refrigerant composition as an optimization variable, which increases both the degrees of freedom and the complexity of solving the thermodynamic model. The new optimization problem minimizes the total $U \times A$ value while maintaining a fixed electrical power of 1278 kW. The optimal solutions for pure N_2 and mixed refrigerant (N_2/CH_4) are named OptimDes II and OptimDes III, respectively. The comparison of both solutions in Tables 11 through 15 reveals that the minimum total $U \times A$ value obtained for N_2/CH_4 is 216.7 kW/K. This value denotes a 20.3% reduction compared to the optimized process that uses pure N_2 as a refrigerant (from

271.9 kW/K in OptimDes II to 216.7 kW/K in OptimDes III). The optimized concentration of CH_4 is 20.5 mol%, corresponding to the saturation state, as shown in Fig. 8 for stream #15.

Table 11. Optimal values of (U×A), flowrate and composition of refrigerant, and minimum temperature difference obtained for the optimal solution and base case ($\dot{W}_{NET}$ =1278 kW)

	This work OptimDes II (Derivate-based Optimization Algorithm)	This work OptimDes III (Derivate-based Optimization Algorithm)	Diff (%)
(U×A) total value (kW/K)	271.9	216.7	(-) 20.3
LNG-1, LNG-2, LNG-3	224.0	166.9	(-) 25.5
E-1, E-2, E-3	47.9	49.7	(+) 3.9
Refrigerant flowrate (kmol/s)	0.254	0.255	(+) 0.4
Composition			
N_2	1.0#	0.795	-
CH_4	0.0	0.205	-
$\Delta Tmin$ (K)	2.0##	2.0##	0.0

fixed value ; ## lower bounds (optimization variable)

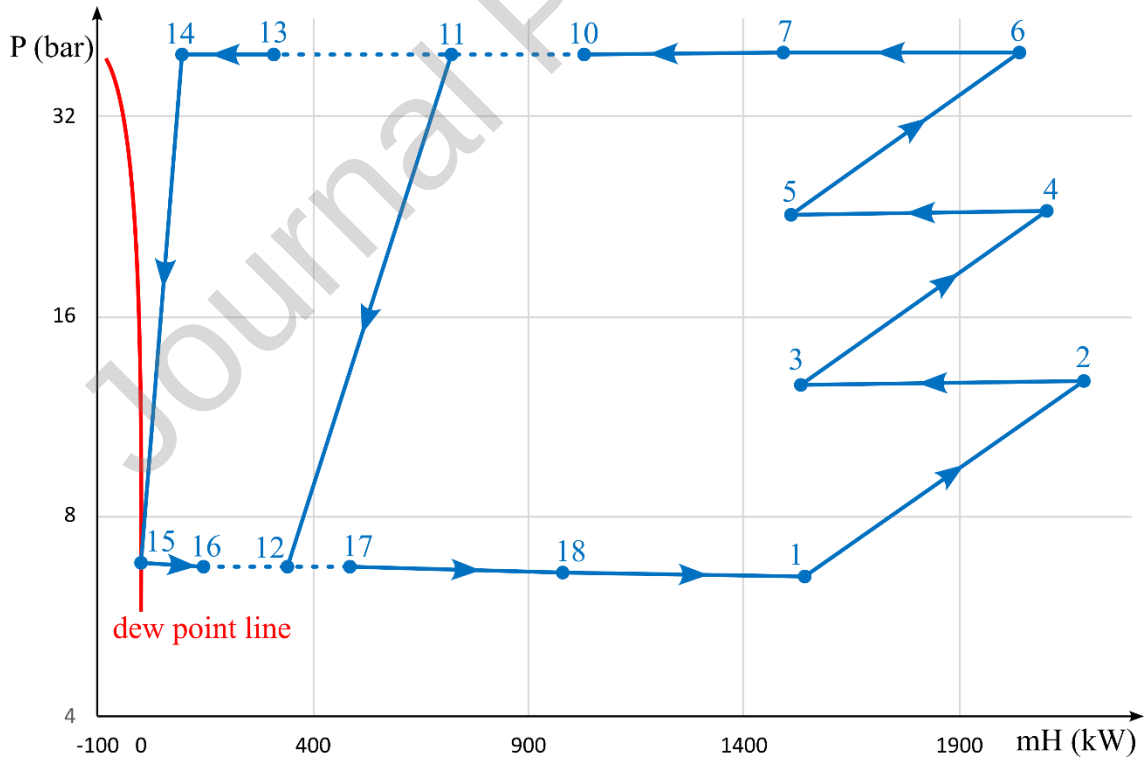

Figure 8. Thermodynamic cycle on a pressure-enthalpy diagram for Case study II.

Table 12 shows that reducing the total $U\times A$ value increases the driving forces (LMTD) required for heat transfer in all heat exchangers, especially in LNG-1, LNG-2, and LNG-3. However, not all these heat exchangers contribute equally to the reduction of the total U×A value. The LNG-1 contribution to the reduction of the total U×A value is not significant, as it only reduces by 1.4 kW/K. However, the largest $U\times A$ decrease is attributed to LNG-2 with 45.1 kW/K decrease (from 112.9 to 67.8 kW/K), and LNG-3 with 10.4 kW/K decrease (from 38.7 to 28.3 kW/K). In OptimDes II and OptimDes III, the heat loads obtained for the LNG-2 and LNG-3 heat exchangers differ by only 1.9%. It should be noted that the LMTD values in OptimDes III are higher (7.2 K vs. 4.4 K in LNG-2 and 5.1 K vs. 3.6 K in LNG-3), which means that the $U\times A$ values are significantly lower compared to OptimDes II.

Table 12. Optimal values obtained for the designs of heat exchangers corresponding to single and mixed refrigerants ($\dot{W}_{NET}$ =1278 kW).

		This work OptimDes II (Derivate-based Optimization Algorithm)	This work OptimDes III (Derivate-based Optimization Algorithm)	Diff (%)
Total heat load (kW)	LNG-1	502.5	561.7	(+) 11.8
	LNG-2	496.7	491.3	(-) 1.1
	LNG-3	141.1	143.9	(+) 1.9
	E-1	652.4	658.2	(+) 0.9
	E-2	595.4	594.3	(-) 0.2
	E-3	550.9	546.2	(-) 0.9
($U\times A$) (kW/K)	LNG-1	72.3	70.9	(-) 2.0
	LNG-2	112.9	67.8	(-) 40.0
	LNG-3	38.7	28.3	(-) 27.0
	E-1	16.8	17.5	(+) 4.3
	E-2	16.3	16.9	(+) 3.9
	E-3	14.8	15.4	(+) 3.5
LMTD (K)	LNG-1	6.9	7.9	(+) 14.1
	LNG-2	4.4	7.2	(+) 64.8
	LNG-3	3.6	5.1	(+) 39.7
	E-1	38.9	37.6	(-) 3.3
	E-2	36.6	35.2	(-) 3.9
	E-3	37.1	35.6	(-) 4.2

Table 13 shows the best power distribution between compressors and expanders to achieve a net power target of 1278 kW. A comparison of the two designs shows that in OptimDes III, both the power

consumption of the compressors and the power generated by the expanders are lower than in OptimDes II (8.2 kW each), indicating a preference for mixed N_2/CH_4 refrigerant instead of single N_2 refrigerant.

Table 13. Optimal values of electrical power required by compressors and generated by expanders obtained by considering single and mixed refrigerants ($\dot{W}_{NET}$ =1278 kW)

		This work OptimDes II (Derivate-based Optimization Algorithm)	This work OptimDes III (Derivate-based Optimization Algorithm)	
				Diff (%)
Compressor (kW)	K-1	642.1	649.4	(+) 1.1
	K-2	578.3	573.1	(-) 0.9
	K-3	539.5	529.2	(-) 1.9
		1759.9	1751.7	(-) 0.5
Expander (kW)	EXP-1	384.9	377.9	(-) 2.0
	EXP-2	97.1	95.8	(-) 0.6
		481.9	473.7	(-) 1.7
$\dot{W}_{NET}$ (kW)		1278	1278	

Table 14. Optimal values of pressure, temperature, and flowrates obtained by considering single and mixed refrigerants ($\dot{W}_{NET}$ =1278 kW).

	This work OptimDes II (Derivate-based Optimization Algorithm)			This work OptimDes III (Derivate-based Optimization Algorithm)		
	T [K]	P [bar]	$\dot{m}$ [kmol/s]	T [K]	P [bar]	$\dot{m}$ [kmol/s]
1	311.2	6.5111	0.25382	310.6	6.508	0.25479
2	397.2	12.678	0.25382	392.5	12.798	0.25479
3	311.2	12.478	0.25382	311.2	12.598	0.25479
4	388.7	22.866	0.25382	383.7	23.021	0.25479
5	311.2	22.666	0.25382	311.2	22.821	0.25479
6	383.5	40.000	0.25382	378.5	40.000	0.25479
7	313.2	39.800	0.25382	313.2	39.800	0.25479
10	261.3	39.700	0.25382	258.0	39.700	0.25479
11	261.3	39.700	0.17860	258.0	39.700	0.17874
12	177.7	6.711	0.17860	176.3	6.708	0.17874
13	261.3	39.700	0.07521	258.0	39.700	0.07605
14	179.7	39.600	0.07521	180.6	39.600	0.07605
15	116.2	6.811	0.07521	116.2	6.808	0.07605
16	177.7	6.711	0.07521	175.5	6.708	0.07605
17	177.7	6.711	0.25382	176.1	6.708	0.25479

18	244.0	6.611	0.25382	239.0	6.608	0.25479
NG	313.2	62.900	0.03667	313.2	62.900	0.03667
20	261.3	62.800	0.03667	258.0	62.800	0.03667
23	179.7	62.700	0.03667	180.6	62.700	0.03667
24	118.2	62.600	0.03667	118.2	62.600	0.03667
25	111.1	1.013	0.03667	111.1	1.013	0.03667

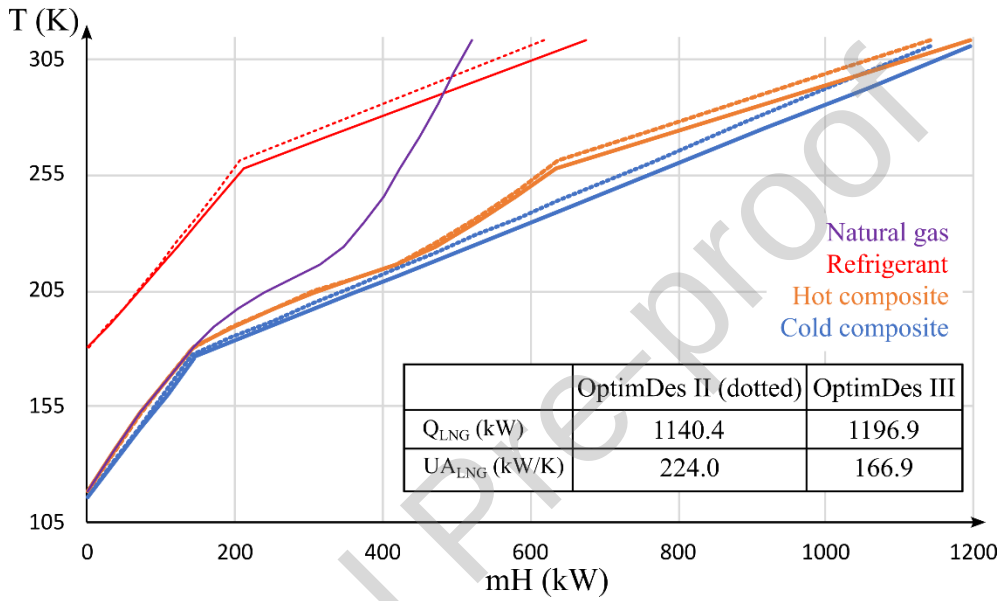

Figure 9. Optimal temperature-enthalpy rate diagrams obtained for single and mixed refrigerants.

Table 15. Comparison of the optimal values for the design of heat exchangers obtained for OptimDes II and OptimDes III ($\dot{W}_{NET}$ =1278 kW)

		q_{LNG} at section k_i (kW)		LMTD at section k_i (K)		(U×A) at section k_i (kW/K)		ΔT at point i (K)		
		OptimDes II	OptimDes III	OptimDes II	OptimDes III	OptimDes II	OptimDes III		OptimDes II	OptimDes III
LNG-1	$k_{i=1}$	125.6	140.4	3.5	4.1	35.8	33.8	i=1	2.0#	2.5
	$k_{i=2}$	125.6	140.4	7.4	8.2	17.1	17.2	i=2	5.6	6.3
	$k_{i=3}$	125.6	140.4	11.2	12.3	11.2	11.4	i=3	9.4	10.3
	$k_{i=4}$	125.6	140.4	15.2	16.6	8.2	8.4	i=4	13.3	14.5
								i=5	17.4	18.9
LNG-2	$k_{i=1}$	55.2	54.6	14.6	16.3	3.8	3.3	i=1	17.4	18.9
	$k_{i=2}$	55.2	54.6	9.6	11.7	5.8	4.7	i=2	12.1	14.0
	$k_{i=3}$	55.2	54.6	5.5	7.9	10.0	6.9	i=3	7.5	9.6
	$k_{i=4}$	55.2	54.6	3.0	5.6	18.3	9.7	i=4	3.9	6.4
	$k_{i=5}$	55.2	54.6	2.7	5.4	20.5	10.1	i=5	2.2	4.9

	$k_{i=6}$	55.2	54.6	4.1	6.7	13.6	8.2	i=6	3.2	5.9
	$k_{i=7}$	55.2	54.6	5.2	7.6	10.5	7.2	i=7	5.1	7.5
	$k_{i=8}$	55.2	54.6	4.7	7.1	11.7	7.7	i=8	5.4	7.7
	$k_{i=9}$	55.2	54.6	2.9	5.4	18.8	10.0	i=9	4.1	6.5
								i=10	2.0#	4.5
LNG-3	$k_{i=1}$	35.3	36.0	3.0	5.9	11.6	6.1	i=1	2.0#	5.1
	$k_{i=2}$	35.3	36.0	4.7	6.8	7.5	5.3	i=2	4.4	6.9
	$k_{i=3}$	35.3	36.0	4.6	5.9	7.7	6.1	i=3	5.0	6.8
	$k_{i=4}$	35.3	36.0	3.0	3.3	12.0	10.9	i=4	4.2	5.1
								i=5	2.0#	2.0#
Total		1140.4	1196.9 (+4.9%)			224	166.9 (-25.5%)			

optimal values reaching the lower bound imposed for ΔT_{MIN}.

The composite curves of both the base and optimized cases are presented in Fig. 9. Adding CH_4 to the N_2 refrigerant impacts the heat transfer across the three LNG heat exchangers. In addition, Table 15 provides details on the optimal values of heat load, temperature difference, and U×A value in each section of the three LNG heat exchangers presented in Figure 9.

As presented in Figure 9, although OptimDes III has a higher heat recovery compared to OptimDes II (1197 kW vs. 1140.4 kW, the total $U \times A$ value is lower by 57 kW/K (166.9 kW/K vs. 224 kW/K). In addition, Table 15 shows that in all points of the three LNG heat exchangers in OptimDes III, except for the last point of LNG-3 where ΔT reached ΔT_{min} = 2 K, ΔT is greater than ΔT_{min}. On the other hand, in OptimDes II, ΔT reached ΔT_{min} = 2 K four times (once in LNG-1 at i=1, once in LNG-2 at i=10, and twice in LNG-3 at i=1 and 5).

Finally, it is noteworthy that the previous case studies were solved without using the preprocessing phase described in the solution strategy. Some cases experienced convergence problems, and thus, solutions could not be reached. This resulted in infeasible solutions with many function evaluation errors and high values for Jacobian matrix elements. In other cases, local solutions showed poor objective values, incorrect heat transfer areas, and electrical power distribution in compressors and expanders. Table 16 illustrates the increase in model size and the change in objective function values during the execution of the initialization phase. Figure 10 shows a comparison of the temperature profiles of Model-2 and Model-3.

Table 3. Number of equations and variables, and objective function values related to the models used in the preprocessing phase.

	Equations (both equality and inequality constraints)	Variables	Objective function					
			OptimDes I		OptimDes II		OptimDes III	
			$\dot{W}_{NET}$	$(U\times A)$	$\dot{W}_{NET}$	$(U\times A)$	$\dot{W}_{NET}$	$(U\times A)$
Model-1	227	199	1266.3	-	1266.3	-	1266.3	-
Model-2	297	310	-	-	-	-	-	-
Model-3	543	438	1277.3	-	1277.3		1277.3	
Model-4	612	507	1277.3	277.4	1278[#]	271.9	1278[#]	216.7

fixed value

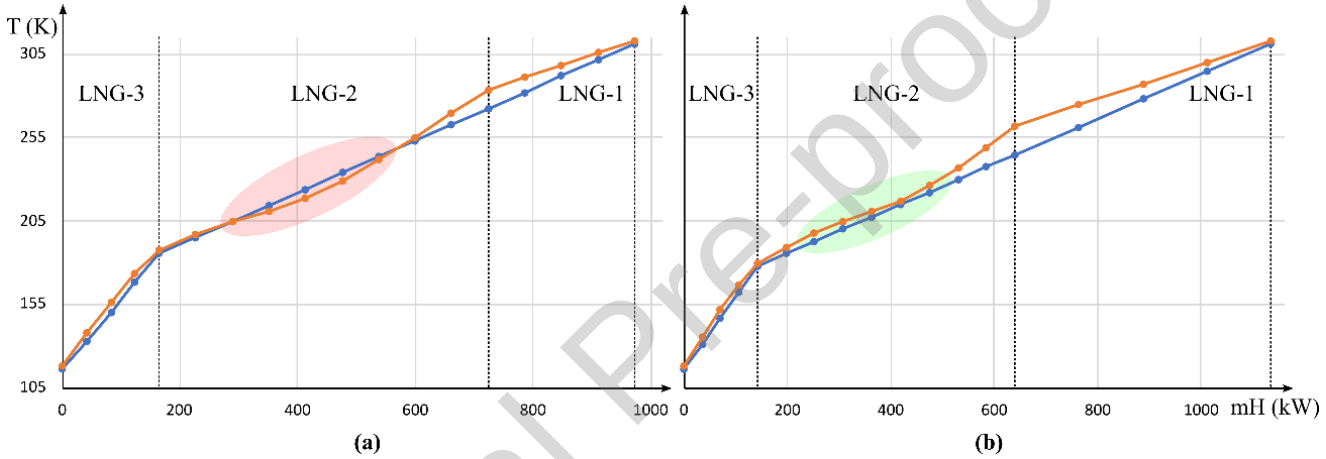

Figure 10. Comparison of temperature profiles within LNG heat exchangers obtained for Model-2 (a) and Model-3 (b).

Table 16 shows that Model-2, which models only the LNG-1, LNG-2, and LNG-3 heat exchangers, requires more equations and variables than Model-1, which accounts for all global mass and energy balances of all process units.

According to Fig. 10a, the simulation obtained from Model-2 shows that certain ΔT values at some points of the LNG-2 heat exchanger do not meet the ΔT_{min} value since Eq. (32) is not considered in this model. The solution of Model 3, which now includes Eq. (32), shows how all ΔT values are conveniently distributed within the exchangers to satisfy ΔT_{min} and optimize the objective function (Figure 10b). Thus, the preprocessing phase is an efficient and systematic procedure for initializing and bounding variables with a minimal number of infeasibilities. By combining this procedure with the robustness of the optimization algorithm used, the approach proves to be sufficiently robust to ensure convergence and find the optimal solution for the more detailed model proposed (Model-4). This procedure can be properly

extended to optimize other processes such as: optimization of design of CO_2 capture processes (Mores et al. 2019), heat exchanger networks (Oliva et al. 2011), wastewater treatment plants (Alasino et al. 2010), liquid hydrogen regasification systems (Incer-Valverde et al. 2023b), cryogenics-based energy storage systems (Incer-Valverde et al. 2021).

Finally, to verify the optimization results presented in this work, simulation runs were executed in Aspen HYSYS (Fig. 11), utilizing the optimal outcomes obtained from the proposed NLP model as input data. In essence, simulation runs were conducted under the optimal conditions determined by the model; the degrees of freedom of the optimization problem were fixed at the optimal values obtained.

Figure 12 illustrates the differences obtained between our model and Aspen HYSYS, concluding that these differences are insignificant. For example, of a total of 507 variables, there are eight variables with differences lower than 1% and two others with differences of 2.2%. These results indicate that the quality of solutions obtained from the proposed model is similar to Aspen HYSYS. Thus, in addition to preserving the calculation quality of HYSYS, the proposed model enables simultaneous optimization, which would be challenging to perform with Aspen HYSYS alone.

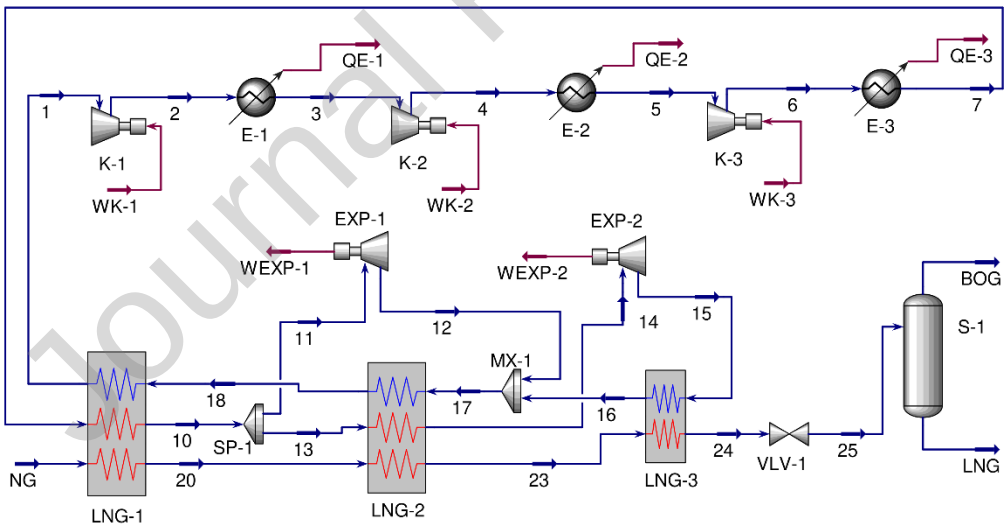

Figure 11. Flowsheet implemented in Aspen HYSYS for verification purposes.

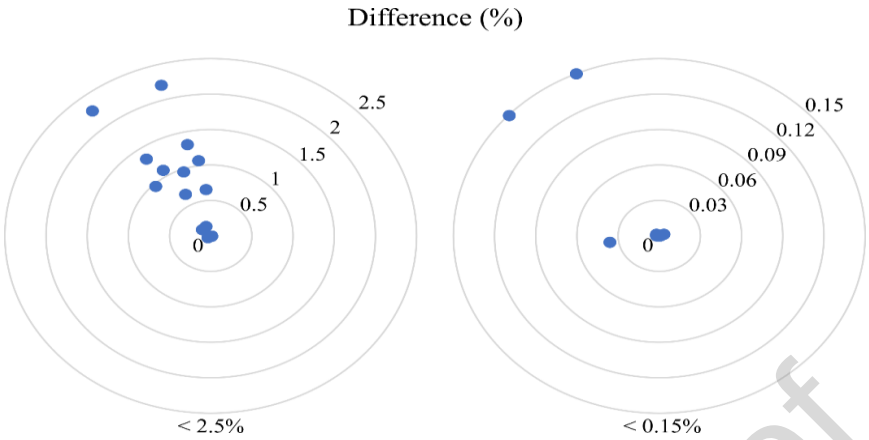

Figure 12. Numerical differences in variables between ASPEN HYSYS and the proposed NLP optimization model.

Conclusions

This paper introduced an optimization framework that couples the advantages of mathematical programming and a dynamic link library (DLL) to optimize the design of LNG liquefaction cycles. The primary objective was to minimize the power consumption for a given configuration of liquefied natural gas.

A nonlinear mathematical model was created and implemented within the General Algebraic Modeling System (GAMS). It was then linked to a DLL coded in the "C" programming language, enabling precise computation of the intricate thermodynamic properties essential for optimization.

Furthermore, a preprocessing phase was proposed to enhance the convergence of the model. This phase involved initializing and bounding all variables.

After successfully verifying the model by comparing its results with a base case from existing literature, it was applied to two case studies. In Case-1, pure N_2 was used as the refrigerant, while in the second in Case-2, a mixture of N_2 and CH_4 was examined, with the mixture composition treated as an optimization variable.

Optimizing Case-2 required solving a more complex model compared to the first, as it involved calculating the thermodynamic properties of the refrigerant mixture. In comparison to previously published results obtained using GA and ASPEN HYSYS, the deterministic approach yielded the following outcomes:

- A significant reduction in electrical power consumption when employing pure N_2 refrigerant. The optimized design led to a 10% reduction in electrical power usage in comparison to the base case, saving 1277 kW instead of 1398 kW.

- Additionally, optimizing the process using a mixture of N_2 and CH_4 resulted in an optimal CH_4 composition of 20.5 mol%, leading to approximately a 20% reduction in the total (U×A) value compared to using pure N_2 as the refrigerant, while maintaining the same electrical power consumption of 1278 kW.

In future research, the proposed nonlinear programming (NLP) model will be expanded to add the optimization of process layout. Consequently, a proposal for simultaneously optimizing operating conditions, sizing, and process layout will be introduced. Incorporating the process layout as an optimization variable in the current model will involve discrete decisions, necessitating the development of either a mixed-integer nonlinear programming (MINLP) model or a generalized disjunctive programming (GDP) model.

Reference

- Alasino, N., Mussati, M.C., Scenna, N.J., Aguirre, P.A., 2010. Wastewater treatment plant synthesis and design: Combined biological nitrogen and phosphorus removal, Industrial and Engineering Chemistry Research, 49 (18), 8601–8612. https://doi.org/10.1021/ie1000482
- Ali, W., Khan, M.S., Qyyum, M.A., Lee M., 2018. Surrogate-assisted modeling and optimization of a natural-gas liquefaction plant, Comp Chem Eng 118, 132–142. https://doi.org/10.1016/j.compchemeng.2018.08.003
- Allahyarzadeh-Bidgoli, A., Dezan, D.J., Yanagihara, J.I., 2018. Optimal design of multistream plate fin heat exchangers used in the cooling stage of a cascade LNG plant, Proceedings of the 16th International Heat Transfer Conference; 5141–5150.
- Almeida-Trasvina, F., Smith, R., 2019. Novel refrigeration cycle configurations for performance improvements in LNG processes at small scale, Comp Aided Chem Eng. Elsevier 46, 421–426. https://doi.org/10.1016/B978-0-12-818634-3.50071-0
- Anteportalatina-García, V.M., Martín, M., 2022. Process synthesis for the valorisation of low-grade heat: Geothermal brines and Industrial waste streams. Renew. Energ. 198, 733–748 https://doi.org/10.1016/j.renene.2022.08.064
- Aspelund, A., Gundersen, T., Myklebust, J., Nowak, M., Tomasgard, A., 2010. An optimization-simulation model for a simple LNG process, Comput Chem Eng. 34, 1606–1617. https://doi.org/10.1016/j.compchemeng.2009.10.018
- Aspen Plus: Getting Started Using Equation Oriented Modeling, Version Number: V8.4, Aspen Technology, 2013.
- Audet, C., Hare, W., 2017. Derivative-free and black box optimization, In: Springer Series in Operations Research and Financial Engineering. 1–300.
- Brodal, E. , Jackson, S., Eiksund, O., 2019. Performance and design study of optimized LNG Mixed Fluid Cascade processes, Energy 189, 116207. https://doi.org/10.1016/j.energy.2019.116207
- Burgard, A., Eason, J., Eslick, J.C., Ghouse, H.J., Lee, A., Biegler, L.T., Miller, C.D., 2018. A Smooth, Square Flash Formulation for Equation-Oriented Flowsheet Optimization, Computer Aided Chemical Engineering, 44, 871–876. https://doi.org/10.1016/B978-0-444-64241-7.50140-3

- Cao, L., Liu, J., Xu, X., 2016. Robustness analysis of the mixed refrigerant composition employed in the single mixed refrigerant (SMR) liquefied natural gas (LNG) process, Appl Therm Eng, 93, 1155–1163. https://doi.org/10.1016/j.applthermaleng.2015.10.072
- Castillo, L., Majzoub Dahouk, M., Di Scipio, S., Dorao, CA., 2013. Conceptual analysis of the precooling stage for LNG processes, Energy Convers Manag, 66, 41–47. https://doi.org/10.1016/j.enconman.2012.09.021
- Chen, X., Li, W., Gong, G., Wan, Z., Tu, Z., 2017. Parametric analysis and optimization of PEMFC system for maximum power and efficiency using MOEA/D, Appl Therm Eng, 121, 400–409. https://doi.org/10.1016/j.applthermaleng.2017.03.144
- Chen, J.J., 2019. Logarithmic mean: Chen's approximation or explicit solution?, Comp Chem Eng, 120, 1–3. https://doi.org/10.1016/j.compchemeng.2018.10.002
- Deiters, U.K., Macias-Salinas, R., 2014. Calculation of densities from cubic equations of state: revisited, Ind Eng Chem Res, 53, 2529–2536. https://doi.org/10.1021/ie4038664
- Ding, H., Sun, H., He, M., 2016. Optimisation of expansion liquefaction processes using mixed refrigerant N2–CH4, Appl Therm Eng, 93, 1053–1060. https://doi.org/10.1016/j.applthermaleng.2015.10.004
- Dowling A., Biegler, L.T., 2015. A framework for efficient large scale equationoriented flowsheet optimization, Comp. Chem Eng, 72, 3–20. https://doi.org/10.1016/j.compchemeng.2014.05.013
- Drud, A.S., 1996. CONOPT: A System for Large Scale Nonlinear Optimization, Reference Manual for CONOPT Subroutine Library, 69 pags., ARKI Consulting and Development A/S, Bagsvaerd, Denmark.
- Edgar, T.F. Himmelblau, D.M. Lasdon, L.S., 2001. Optimization of chemical processes, McGraw Hill Chemical Engineering Series, New York; 2001.
- Esche, E., Weigert, J., Rihm, G.B., Göbel, J., Repke, J.U., 2022. Architectures for neural networks as surrogates for dynamic systems in chemical engineering, Chemical Engineering Research and Design, 177, 184–199. https://doi.org/10.1016/j.cherd.2021.10.042.
- Forster, T., Vázquez D., Guillén-Gosálbez, G., 2023. Algebraic surrogate-based process optimization using Bayesian symbolic learning, AIChE J. 69,e18110. https://doi.org/10.1002/aic.18110
- GAMS Development Corporation. General Algebraic Modeling System (GAMS) Release 36.1.0, Fairfax, VA, USA, 2021.
- Ghorbani, B., Mafi, M., Shirmohammadi, R., Hamedi, M.H., Amidpour, M., 2014. Optimization of operation parameters of refrigeration cycle using particle swarm and NLP techniques, J Nat Gas Sci Eng, 21, 779–790. https://doi.org/10.1016/j.jngse.2014.10.007
- He, T., Karimi, I., Ju, Y., 2018. Review on the design and optimization of natural gas liquefaction processes for onshore and offshore applications, Chem Eng Res Des, 132, 89–114. https://doi.org/10.1016/j.cherd.2018.01.002
- Henao, C.A., Maravelias, C.T., 2023. Surrogate-Based Superstructure Optimization Framework, AIChE J., 57(5), 1216–1232. https://doi.org/10.1002/aic.12341
- Hu, Q., Shan, W., Zhang, W., Li, Y., Wang, W., Zhu, J., Liu, Y., Xie, B., Yu, X., 2021. Optimization and experiment on the dual nitrogen expansion liquefaction process with pre-cooling, Cryogenics, 114, 103243. https://doi.org/10.1016/j.cryogenics.2020.103243
- Hwang, J.H., Roh, M.I., Lee, K.Y., 2013. Determination of the optimal operating conditions of the dual mixed refrigerant cycle for the LNG FPSO topside liquefaction process, Comp Chem Eng, 49, 25–36. https://doi.org/10.1016/j.compchemeng.2012.09.008
- IEA, World Energy Outlook, International Energy Agency, Paris, 2022.

- IEA, Gas Market Report, Q3-2022. Including Gas 2022 medium-term forecast to 2025, International Energy Agency, Paris, 2022. https://www.iea.org/reports/gas-market-report-q3-2022/executive-summary.
- Incer-Valverde, J., Mörsdorf, J., Morosuk, T., Tsatsaronis, G., 2023a. Power-to-liquid hydrogen: Exergy-based evaluation of a large-scale system, International Journal of Hydrogen Energy, 48, 11612–11627. https://doi.org/10.1016/j.ijhydene.2021.09.026
- Incer-Valverde, J., Lugo-Mayor, C., Tsatsaronis, G., Morosuk, T., 2023b. Evaluation of the large-scale hydrogen supply chain and perspectives on LH2 regasification cogeneration systems, Gas Science and Engineering, 115, 205005. https://doi.org/10.1016/j.jgsce.2023.205005
- Incer-Valverde, J., Hamdy, S., Morosuk, T., Tsatsaronis, G., 2021. Improvement perspectives of cryogenics-based energy storage, Renewable Energy, vol. 169, pp. 629–640. https://doi.org/10.1016/j.renene.2021.01.032
- International Gas Union (IGU), World LNG report 2023, https://www.igu.org/
- Jin, C., Lim, Y., 2019. Optimization and economic evaluation of integrated natural gas liquids (NG0L) and liquefied natural gas (LNG) processing for lean feed gas, Appl Therm Eng, vol. 149, 1265–1273. https://doi.org/10.1016/j.applthermaleng.2018.12.143
- Kamath, R.S., Biegler, L.T., Grossmann, I.E., 2010. An equation-oriented approach for handling thermodynamics based on cubic equation of state in process optimization, Comp Chem Eng, 34, 2085–2096. https://doi.org/10.1016/j.compchemeng.2010.07.028
- Kang, C.A., Brandt, A.R., Durlofsky L.J., 2016. A new carbon capture proxy model for optimizing the design and time-varying operation of a coal-natural gas power station. Int J Greenh Gas Control, 48, 234–52. https://doi.org/10.1016/j.ijggc.2015.11.023
- Kang, Y., Luo Y., Yuan, X., 2022. Recent progress on equation-oriented optimization of complex chemical processes, Chinese Journal of Chemical Engineering, 41, 162–169. https://doi.org/10.1016/j.cjche.2021.10.018
- Kazemian, M.E., Gandjalikhan Nassab, S.A., 2020. Thermodynamic Analysis and Statistical Investigation of Effective Parameters for Gas Turbine Cycle using the Response Surface Methodology. *Int. J. Eng.*, *33*, 894–905.
- Kesgin, U., Heperkan, H., 2005. Simulation of thermodynamic systems using soft computing techniques. Int J Energy Res, 29, 581–611. https://doi.org/10.1002/er.1095
- Keshavarzian, S., Gardumi, F., Rocco, M.V., Colombo, E., 2016. Off-design modeling of Natural Gas Combined Cycle power plants: An order reduction by means of Thermoeconomic Input-Output Analysis. Entropy, 18(3), 71. https://doi.org/10.3390/e18030071
- Khan, M. S., Husnil, Y. A., Kwon, Y. S., Lee, M., 2011. Automated optimization of process plant using particle swarm optimization, International Symposium on Advanced Control of Industrial Processes (ADCONIP 2011), Hangzhou, China, 615–620.
- Khan, M.S., Lee, M., 2013. Design optimization of single mixed refrigerant natural gas liquefaction process using the particle swarm paradigm with nonlinear constraints, Energy, 49, 146–155. https://doi.org/10.1016/j.energy.2012.11.028
- Khan, M.S., Karimi, I.A., Lee M., 2016. Evolution and optimization of the dual mixed refrigerant process of natural gas liquefaction, Applied Thermal Engineering, 96, 320–329. https://doi.org/10.1016/j.applthermaleng.2015.11.092.
- Khan, M., Karimi, I., Wood, D., 2017. Retrospective and future perspective of natural gas liquefaction and optimization technologies contributing to efficient LNG supply: A review, J Nat Gas Sci Eng, 45, 165–188. https://doi.org/10.1016/j.jngse.2017.04.035

- Kim, S., Mun-Gi Jang, Jin-Kuk Kim, 2023. Process design and optimization of single mixed-refrigerant processes with the application of deep reinforcement learning, Appl Therm Eng, 223, 120038. https://doi.org/10.1016/j.applthermaleng.2023.120038
- Javaloyes-Antón, J., Kronqvist, J., Caballero, J.A., 2022. Simulation-based optimization of distillation processes using an extended cutting plane algorithm, Computers & Chemical Engineering, 159, 107655. https://doi.org/10.1016/j.compchemeng.2021.107655
- Lee, G.C., Smith, R., Zhu, X.X., 2002. Optimal synthesis of mixed-refrigerant systems for low-temperature processes, Ind Eng Chem Res, 41, 5016–5028. https://doi.org/10.1021/ie020057p
- Li, H., Liao, Z., Sun, J., Jiang, B., Wang, J., Yang, Y., 2020. Simultaneous design of hydrogen allocation networks and PSA inside refineries. Ind. Eng. Chem. Res., 59(10), 4712–4720. https://doi.org/10.1021/acs.iecr.9b06955
- Li, M., Zhuang,Y., Li, W., Dong, Y., Zhang, L., Du, J., Shengqiang, S., 2021. A surrogate-based optimization framework for simultaneous synthesis of chemical process and heat exchanger network, Chemical Engineering Research and Design, 170, 180–188. https://doi.org/10.1016/j.cherd.2021.04.001
- Liu, Z., Romagnoli, A., Sapin, P., Markides, C., Mersch, M., 2021. Dynamic control strategies for a solar-ORC system using first-law dynamic and data-driven machine learning models. 6th International Seminar on ORC Power Systems, October 11-13, 2021, Munich, Germany.
- Lobo, F.G., Lima, C.F., Michalewicz, Z., 2007. Parameter Setting in Evolutionary Algorithms. ISBN 978-3-540-69225-6. Vol. 54.
- Manassaldi, J.I., Mussati, M.C., Scenna, N.J., Mussati, S.F., 2019. Development of extrinsic functions for optimal synthesis and design—Application to distillation-based separation processes, Comp Chem Eng, 125, 532–544. https://doi.org/10.1016/j.compchemeng.2019.03.028
- Matovu, F., Mahadzir, S., Ahmed, R., Mohammad Rozali, N.E., 2022. Synthesis and optimization of multilevel refrigeration systems using generalized disjunctive programming, Comp Chem Eng, 163,107856. https://doi.org/10.1016/j.compchemeng.2022.107856
- Mehrpooya, M., Esfilar, R., Moosavian, S.A., 2017. Introducing a novel air separation process based on cold energy recovery of LNG integrated with coal gasification, transcritical carbon dioxide power cycle and cryogenic CO2 capture, J Clean Prod 142, 1749–1764. https://doi.org/10.1016/j.jclepro.2016.11.112
- Mencarelli, L., Pagot, A., Duchêne, P., 2020. Surrogate-based modeling techniques with application to catalytic reforming and isomerization processes, Computers and Chemical Engineering, 135, 106772. https://doi.org/10.1016/j.compchemeng.2020.106772.
- Moein, P., Sarmad, M., Ebrahimi, H., Zare, M., Pakseresht, S., Vakili, S., 2015. APCI-LNG single mixed refrigerant process for natural gas liquefaction cycle: Analysis and optimization, J Nat Gas Sci Eng, 26, 470–479. https://doi.org/10.1016/j.jngse.2015.06.040
- Mores, P.L., Arias, A.M., Scenna, N.J., Mussati, M.C., Mussati, S.F., 2019. Cost-based comparison of multi-stage membrane configurations for carbon capture from flue gas of power plants, International Journal of Greenhouse Gas Control, 86, pp. 177–190. https://doi.org/10.1016/j.ijggc.2019.04.021
- Oliva, D.G., Francesconi, J.A., Mussati, M.C., Aguirre, P.A., 2011. Modeling, synthesis and optimization of heat exchanger networks. Application to fuel processing systems for PEM fuel cells, International Journal of Hydrogen Energy, 36 (15), 9098–9114.
https://doi.org/10.1016/j.ijhydene.2011.04.097
- Palagi, L., Sciubba, E., Tocci, L., 2019. A neural network approach to the combined multi-objective optimization of the thermodynamic cycle and the radial inflow turbine for Organic Rankine cycle applications, Applied Energy, 237(C), 210–226. https://doi.org/10.1016/j.apenergy.2019.01.035
- Pattison, C.R., Baldea, M., 2015. Multistream heat exchangers: Equation-oriented modeling and flowsheet optimization, AIChE J, 61, 1856–1866. https://doi.org/10.1002/aic.14766

- Primabudi, E. , Morosuk, T., Tsatsaronis, G., 2019. Multi-objective optimization of propane pre-cooled mixed refrigerant (C3MR) LNG process, Energy, 185, 492–504. https://doi.org/10.1016/j.energy.2019.07.035
- Quirante, N., Caballero, J.A., 2016. Large scale optimization of a sour water stripping plant using surrogate models. Computer and Chemical Engineering. 92, 143–162. https://doi.org/10.1016/j.compchemeng.2016.04.039
- Qyyum, M.A., Qadeer, K., Lee, S., Lee, M., 2018a. Innovative propane-nitrogen two-phase expander refrigeration cycle for energy-efficient and low-global warming potential LNG production, Appl. Therm. Eng. 139, 157–165. https://doi.org/10.1016/j.applthermaleng.2018.04.105
- Qyyum, M.A., Long, N.V.D., Minh, L.Q., Lee, M., 2018. Design optimization of single mixed refrigerant LNG process using a hybrid modified coordinate descent algorithm, Cryogenics 89, 131–140. https://doi.org/10.1016/j.cryogenics.2017.12.005
- Ramírez-Márquez, C., Martín-Hernández, E., Martín, M., Segovia-Hernández, J.G., 2020. Surrogate based optimization of a process of polycrystalline silicon production, Computers and Chemical Engineering, 140, 106870. https://doi.org/10.1016/j.compchemeng.2020.106870.
- Riboldi, L., Nords, L.O., 2018. Optimal Design of Flexible Power Cycles through Kriging-based Surrogate Models. Proceedings of ASME Turbo Expo 2018 Turbomachinery Technical Conference and Exposition GT2018 June 11-15, 2018, Oslo, Norway
- Rúa, J., Agromayor, R., Hillestad, M., Nord, L.O., 2020. Optimal dynamic operation of natural gas combined cycles accounting for stresses in thick-walled components, Applied Thermal Engineering, 170, 114858. https://doi.org/10.1016/j.applthermaleng.2019.114858
- Ruiz-Femenia, R., Javaloyes-Antón, J., Salcedo-Díaz, R., Ravagnani, M.A.S.S., Caballero, J.A., 2020. Integration of Chemical Process Simulators with Algebraic Modeling Languages, Editor(s): Sauro Pierucci, Flavio Manenti, Giulia Luisa Bozzano, Davide Manca, Computer Aided Chemical Engineering, Elsevier, 48, 1891-1896. https://doi.org/10.1016/B978-0-12-823377-1.50316-5
- Santos, L.F., Caliane B.B. Costa, C.B.B., Caballero, J.A., Ravagnani, M.A.S.S., 2023. Multi-objective simulation–optimization via kriging surrogate models applied to natural gas liquefaction process design, Energy, 262(Part B), 125271. https://doi.org/10.1016/j.energy.2022.12527
- Santos, L.F., Costa, C.B.B., Caballero, J.A., Ravagnani, M.A.S.S., 2021. Kriging-assisted constrained optimization of single-mixed refrigerant natural gas liquefaction process, Chem Eng Sci, 241,116699. https://doi.org/10.1016/j.ces.2021.116699
- Santos-Rodriguez, M.M., Flores-Tlacuahuac, A., Zavala, V.M., 2017. A stochastic optimization approach for the design of organic fluid mixtures for low-temperature heat recovery, App. Energy, 198, 145–159. https://doi.org/10.1016/j.apenergy.2017.04.047
- Shin, J., Yoon, S., Kim, J.K., 2015. Application of exergy analysis for improving energy efficiency of natural gas liquids recovery processes, Appl Therm Eng, 75, 967–977. https://doi.org/10.1016/j.applthermaleng.2014.10.042
- Soave, G., 1993. Improving the Treatment of Heavy Hydrocarbons by the SRK EOS, Fluid Phase Equilib, 84, 339–342. https://doi.org/10.1016/0378-3812(93)85131-5
- Vikse, M., Watson, H., Kim, D., Barton, P., Gundersen, T., 2020, optimization of a dual mixed refrigerant process using a nonsmooth approach, Energy, 196, 116999. https://doi.org/10.1016/j.energy.2020.116999
- Vilasboas, I., Sousa Fagundes dos Santos, V.G., Ribeiro, A., Silva, J.A.M., 2021. Surrogate Models Applied to Optimized Organic Rankine Cycles, Energies, 14(24), 8456. https://doi.org/10.3390/en14248456

- Wang, M., Zhang, J., Xu, Q., 2012. Optimal design and operation of a C3MR refrigeration system for natural gas liquefaction, Comp Chem Eng, 39, 84–95. https://doi.org/10.1016/j.compchemeng.2011.12.003
- Watson, H.A.J., Khan, K.A., Barton, P.I., 2015. Multistream heat exchanger modeling and design, AIChE J, 61, 3390–3403. https://doi.org/10.1002/aic.14965
- Yadav, S., Banerjee, R., Seethamraju, S., 2022. Thermodynamic Analysis of LNG Regasification Process, Chemical Engineering Transactions, 94, 919–924. DOI:10.3303/CET2294153.
- Xu, X., Liu, J., Jiang, C., Cao, L., 2013. The correlation between mixed refrigerant composition and ambient conditions in the PRICO LNG process, Appl Energy, 102, 1127–1136. https://doi.org/10.1016/j.apenergy.2012.06.031
- Yoon, S., Cho, H., Lim, D.H., Kim, J.K., 2012. Process design and optimization of natural gas liquefaction processes, Chem Eng Trans, 29, 1585–1590. https://doi.org/10.3303/CET1229265
- Yin, L., Ju, Y., 2020. Conceptual design and analysis of a novel process for BOG re-liquefaction combined with absorption refrigeration cycle, Energy, 205, 118008. https://doi.org/10.1016/j.energy.2020.118008.
- Yu, H., Eason, J., Biegler, L.T., Feng, X., 2017. Process integration and superstructure optimization of OrganicRankine Cycles (ORCs) with heat exchanger network synthesis, Comp. Chem. Eng. 107, 257–270. https://doi.org/10.1016/j.compchemeng.2017.05.013
- Zhang, J., Meerman, H., Benders, R., Faaij, A., 2020. Technical and economic optimization of expander-based small-scale natural gas liquefaction processes with absorption precooling cycle, Energy 191, 116592. https://doi.org/10.1016/j.energy.2019.116592

Declaration of Competing Interest

X The authors declare that they have no known competing financial interests or personal relationships that could have appeared to influence the work reported in this paper.

☐The authors declare the following financial interests/personal relationships which may be considered as potential competing interests:

Highlights

- A modeling framework for optimizing LNG processes is provided.

- Dynamic link libraries with an optimization software program are coupled.

- A rigorous thermodynamic model was implemented for optimization.

- The proposed equation-based method handles the nonlinearities of the model.

- The proposed initialization phase assures the convergence of the optimization model.